



HAL
open science

Splicing efficiency of minor introns in a mouse model of SMA predominantly depends on their branchpoint sequence and can involve the contribution of major spliceosome components

Valentin Jacquier, Manon Prévot, Thierry Gostan, Rémy Bordonné, Sofia Benkhelifa-Ziyyat, Martine Barkats, Johann Soret

► To cite this version:

Valentin Jacquier, Manon Prévot, Thierry Gostan, Rémy Bordonné, Sofia Benkhelifa-Ziyyat, et al.. Splicing efficiency of minor introns in a mouse model of SMA predominantly depends on their branchpoint sequence and can involve the contribution of major spliceosome components. *RNA*, 2022, 28 (3), pp.303-319. 10.1261/rna.078329.120 . hal-03687098

HAL Id: hal-03687098

<https://hal.science/hal-03687098>

Submitted on 21 Jul 2022

HAL is a multi-disciplinary open access archive for the deposit and dissemination of scientific research documents, whether they are published or not. The documents may come from teaching and research institutions in France or abroad, or from public or private research centers.

L'archive ouverte pluridisciplinaire **HAL**, est destinée au dépôt et à la diffusion de documents scientifiques de niveau recherche, publiés ou non, émanant des établissements d'enseignement et de recherche français ou étrangers, des laboratoires publics ou privés.

1 **Splicing efficiency of minor introns in a mouse model of SMA**
2 **predominantly depends on their branchpoint sequence and can involve the**
3 **contribution of major spliceosome components.**

4 **Valentin Jacquier¹, Manon Prévot¹, Thierry Gostan¹, Rémy Bordonné¹, Sofia**
5 **Benkhelifa-Ziyyat², Martine Barkats² and Johann Soret^{1,*}**

6 ¹Institut de Génétique Moléculaire de Montpellier, Univ Montpellier, CNRS, Montpellier,
7 France. ²Centre de Recherche en Myologie (CRM), Institut de Myologie, Sorbonne
8 Universités, UPMC Univ Paris 06, Inserm UMR5974, GH Pitié Salpêtrière, Paris 75013,
9 France.

10

11 *To whom correspondence should be addressed. Tel : (+33) 04 34 35 96 84 ; Fax : (+33) 04
12 34 35 96 34 ; Email : johann.soret@igmm.cnrs.fr

13 **ABSTRACT**

14 Spinal Muscular Atrophy (SMA) is a devastating neurodegenerative disease caused by
15 reduced amounts of the ubiquitously expressed Survival of Motor Neuron (SMN) protein. In
16 agreement with its crucial role in the biogenesis of spliceosomal snRNPs, SMN-deficiency is
17 correlated to numerous splicing alterations in patient cells and various tissues of SMA mouse
18 models. Among the snRNPs whose assembly is impacted by SMN-deficiency, those involved
19 in the minor spliceosome are particularly affected. Importantly, splicing of several, but not all
20 U12-dependent introns has been shown to be affected in different SMA models. Here, we
21 have investigated the molecular determinants of this differential splicing in spinal cords from
22 SMA mice. We show that the branchpoint sequence (BPS) is a key element controlling
23 splicing efficiency of minor introns. Unexpectedly, splicing of several minor introns with
24 suboptimal BPS is not affected in SMA mice. Using *in vitro* splicing experiments and
25 oligonucleotides targeting minor or major snRNAs, we show for the first time that splicing of
26 these introns involves both the minor and major machineries. Our results strongly suggest that
27 splicing of a subset of minor introns is not affected in SMA mice because components of the
28 major spliceosome compensate for the loss of minor splicing activity.

29

30 **INTRODUCTION**

31 Spinal Muscular Atrophy is an autosomal recessive disease characterized by both
32 degeneration of motor neurons from the anterior horn of the spinal cord and skeletal muscle
33 atrophy (Pearn 1978, Crawford and Pardo 1996). This leading cause of infant mortality is
34 classified into four types according to the age of onset and clinical severity (Sendtner 2001,
35 Talbot and Davies 2001, Frugier et al. 2002, Monani 2005, Sumner 2006). In all patients, the
36 disease results from homozygous deletions or mutations in the survival motor neuron gene
37 (*SMN1*) but its severity is inversely correlated to the number of copies of the nearly identical
38 gene called *SMN2* (Lefebvre et al. 1995, 1997). Indeed, because of an exonic splicing
39 mutation (Cartegni and Krainer 2002, Kashima and Manley 2003), *SMN2* transcripts
40 preferentially splice out exon 7 and produce a truncated and very unstable protein (Burnett et
41 al. 2009, Cho and Dreyfuss 2010). As a consequence, *SMN2* only expresses low levels of
42 functional SMN protein, accounting for the observation that multiple *SMN2* are required to
43 compensate for the loss of *SMN1* (Lefebvre et al. 1997, Coover et al. 1997, McAndrew et al.
44 1997).

45 SMN is an ubiquitously expressed protein that is essential for viability from yeast to
46 human (Schrank et al. 1997, Wang and Dreyfuss 2001, Paushkin et al. 2002, Campion et al.
47 2010). It has been implicated in many cellular processes including transcription (Pellizzoni et
48 al. 2001), pre-mRNA splicing (Fischer et al. 1997, Pellizzoni et al. 1998), biogenesis of small
49 nucleolar RNPs (Charroux et al. 2000, Pellizzoni et al. 2001, Whitehead et al. 2002) and
50 axonal mRNA transport (Pagliardini et al. 2000, Rossoll et al. 2003, Zhang et al. 2003,
51 Jablonka et al. 2004, Fallini et al. 2011, 2012, Rago et al. 2013, Rihan et al. 2017). However,
52 the best characterized function of SMN is currently as part of a multi-protein complex
53 required for the biogenesis of small nuclear ribonucleoproteins particles (snRNPs) which are
54 components of the splicing machinery (Meister et al. 2001, Pellizzoni et al. 2002). In the

55 cytoplasm, the SMN complex composed of Gemin 2-8 and Unrip assembles a heptameric ring
56 of Sm proteins on each RNA polymerase II-transcribed U-rich snRNA (U1, U2, U4, U4atac,
57 U5, U11 and U12) in order to form a mature snRNP (Charroux et al. 2000, Meister et al.
58 2001, Pellizzoni et al. 2002), this being a prerequisite for import of snRNPs in the nucleus
59 (Pellizzoni 2007) where the splicing reaction occurs. In agreement with the fundamental role
60 of SMN in snRNP biogenesis, it has been shown that extracts of SMA patient cells have a
61 lower snRNPs assembly efficiency, in correlation with their level of functional SMN protein
62 (Wan et al. 2005). Taken together, these observations led to propose that SMA is caused, at
63 least in part, by perturbations of the snRNPs biogenesis, leading to splicing defects of specific
64 mRNAs involved in motor neuron functions. Consistent with this, Gabanella et al. have
65 reported a strong impairment of snRNP assembly in various tissues of a severe SMA mouse
66 model (Gabanella et al. 2007). They showed that defective SMN complex function results in a
67 significant decrease in the levels of a subset of snRNPs and predominantly alters the levels of
68 the U11 snRNP which is a component of the minor spliceosome responsible for the splicing
69 of a rare class of introns (Turunen et al. 2013). Using a moderate SMA mouse model, Zhang
70 et al. have confirmed that SMN deficiency alters the stoichiometry of both major and minor
71 snRNAs and causes widespread pre-mRNA splicing defects in SMA mouse tissues such as
72 spinal cord, liver and kidney (Zhang et al. 2008). In a previous study, we have examined the
73 snRNP repertoire in lymphoblasts from a type I SMA patient and noted a slight decrease of
74 U4atac and U6atac snRNAs in these SMN-deficient cells (Boulisfane et al. 2011).
75 Interestingly, we also observed that the formation of the minor U4atac/U6atac/U5 snRNP is
76 hindered in the SMA cells and that this defect is correlated to a significant splicing inhibition
77 of some, but not all, minor introns (Boulisfane et al. 2011). Accordingly, it has been reported
78 that SMN deficiency impairs splicing of a subset of U12 introns in *Drosophila* larvae,
79 supporting the notion that minor introns are differentially processed when the level of minor
80 snRNPs is decreased (Lotti et al. 2012). More recently, other studies using different SMA
81 models have confirmed that splicing of all minor introns is not similarly affected upon SMN
82 deficiency (Custer et al. 2016, Doktor et al. 2017, Jangi et al. 2017).

83 In the present study, we sought to decipher the molecular bases of the differential
84 splicing defects of minor introns in the SMA context. Using spinal cords of a SMA mouse
85 model, we show that the branchpoint sequence (BPS) of minor introns is a key determinant of
86 splicing efficiency in SMA cells. We also observed that splicing of several minor introns,
87 whose BPS significantly diverges from the consensus motif, is not affected in SMA mice.
88 Since these motifs bear some resemblance with major branchpoint sequences, we have used
89 minor splicing reporters to investigate the role of the major spliceosome in the splicing of
90 minor introns. Altogether, our studies indicate that splicing of a subset of minor introns can
91 depend on both the minor and major splicing machineries.

92

93 **RESULTS**

94 **Minor introns are differentially spliced in SMA mice spinal cords.**

95 To investigate the splicing efficiency of minor introns in a moderately severe mouse
96 model of SMA (Le et al. 2005), we collected spinal cords from 3 SMA (KO6, KO9, KO10)
97 and 2 control mice (WT6, WT7) sacrificed at postnatal day 12 or 13. Splicing efficiency of

98 30-40 minor introns listed in the U12 database (U12DB, [http://genome.crg.es/cgi-](http://genome.crg.es/cgi-bin/u12db/u12db.cgi)
99 [bin/u12db/u12db.cgi](http://genome.crg.es/cgi-bin/u12db/u12db.cgi), Alioto 2007) was analyzed by RT-PCR experiments performed with
100 primers allowing the simultaneous amplification of both spliced and unspliced RNA species.
101 As already observed in previous studies (Boulisfane et al. 2011, Lotti et al. 2012, Custer et al.
102 2016, Doktor et al. 2017, Jangi et al. 2017), some minor introns were significantly retained in
103 spinal cords of SMA mice, as compared to the wild type samples (Mapk9, Ints4, Mapk11;
104 Figure 1A and 1C), whereas splicing of others was not affected (Derl2a, Ppp2r2b, Ppp2r2c;
105 Figure 1B and 1C).

106

107 **Splice donor sequence and intron size are not critical for minor introns retention.**

108 In order to identify the molecular determinants responsible for this differential processing
109 efficiency, we first focused on the sequence of the splice donor site. The U11 consensus
110 sequence for the donor site (RTATCCTTT) is highly conserved and distinct from the U1
111 consensus (GTRAGT; Dietrich et al. 1997). We observed that splicing of minor introns
112 containing perfect consensus donor sequences was either not affected (Mapk1, Vezt; Figure
113 2A and 2E) or significantly impaired (Ppp2r2d, Cip2a; Figure 2B and 2E) regardless of the
114 donor subtype (GT or AT). Similar results were obtained for minor introns containing splice
115 donor sequences divergent from the consensus motif. Their splicing was either not affected
116 (Ncbp2, Gpaa1; Figure 2C and 2E) or significantly inhibited (Gbl, Nup210; Figure 2D and
117 2E). These observations indicate that the sequence of the splice donor site is not the primary
118 determinant for the minor introns differential splicing in SMA mice.

119 To determine whether the size of the intron could influence the splicing process, we then
120 analyzed the splicing efficiency of minor introns of various lengths. For short introns, some
121 such as Mapk11 (198nt; Figure 1) were clearly affected in SMA spinal cords, whereas other
122 such as Gpaa1 (176nt; Figure2) were not retained. Differential splicing efficiency was also
123 observed for longer introns (>1.0kb) which were either slightly/not affected such as Derl2a
124 (1082nt; Figure 1) or significantly retained such as Ppp2r2d (1067nt; Figure 2), indicating
125 thereby that intron size is neither responsible for the observed differential intron retention.

126

127 **Branchpoint sequence is a key determinant for minor intron retention in SMA mice.**

128 Minor introns share a highly conserved branchpoint sequence (BPS, TTCCTTRAY, Hall and
129 Padgett 1994, Alioto 2007) which serves as a primary recognition sequence for the U12
130 snRNA. To determine whether the sequence of BPS could be involved in the differential
131 splicing of minor introns in the spinal cords of SMA mice, we analyzed the splicing efficiency
132 of minor introns containing consensus or divergent branchpoint sequences. As shown in
133 Figure 3A and 3C, the splicing of introns containing consensus BPS (Ddx54, Ppp2r2b and
134 Slc12a4) was not significantly inhibited in SMA samples compared to wild-type, whereas the
135 retention of introns diverging from the consensus by only one or more nucleotides (Plcb2,
136 Ncbp1 and Vps16b) was increased by ~2 to 3.5 times (Figure 3B and 3C).

137 To confirm these results, we first determined the U12 binding energy for each of the
138 142 different branchpoint sequences identified in the 555 murine minor introns compiled in
139 the U12 database. This was performed as described in Mercer et al. (Mercer et al. 2015) by
140 calculating the number of hydrogen bonds between the branchpoint motifs and the
141 branchpoint binding sequence of the U12 snRNA. We then examined the splicing efficiency

142 of several minor introns differing by the score of their BPS (see Table 1). As expected,
143 Ddx54, Ppp2R2b, Slc12a4 (Figure 3A and 2C) as well as Pten, Srpk1 and Usp14 introns
144 (Figure 4A and 4C) whose BPS corresponds to the TTCCTTRAY consensus and exhibits the
145 highest scores (19 and 18) are spliced almost as efficiently in WT and SMA spinal cords. As
146 already observed (Figure 3B and 3C), the splicing efficiency is clearly affected in SMA mice
147 when the BPS score decreases as shown for Plcb2, Ncbp1 and Vps16b introns in Figure 3
148 (BPS score = 13, 17 and 17, respectively) or for Ap4e1, Ncoa6ip and Vac14 introns in Figure
149 4 (BPS score = 16, 15 and 12, respectively).

150 Altogether, these observations indicate that minor introns with optimal BPS are not
151 significantly affected in SMN-deficient cells and suggest that suboptimal branchpoint regions
152 are correlated to an increase of minor introns retention in response to SMN depletion.

153

154 **Splicing of a subset of minor introns containing a suboptimal BPS is not inhibited upon** 155 **SMN deficiency.**

156 Our analysis of the splicing efficiency of introns containing suboptimal BPSs revealed
157 however that if some of them (Derl2b, Exosc1, Ints7; Figure 5A and 5C) are clearly affected
158 in SMN-deficient spinal cords, other (Llglh, Gosr1, Tsta3; Figure 5B and 5C) appear to be
159 insensitive to SMN deficiency. Careful examination of the branch sequences contained in the
160 unaffected introns pointed to an increased capacity to interact with the U2 snRNA, thereby
161 suggesting that components of the major spliceosome could compensate for the biogenesis
162 defects of minor snRNPs in SMA mice. To address this possibility, we re-examined the 142
163 minor BPSs for their complementarity with the corresponding anti-branch sequence (5'-
164 GTAGTATC-3') of the U2 snRNA. In major introns, the GTAGTA motif binds to the
165 TRYTRAY sequence surrounding the branchpoint nucleotide (underlined; Taggart et al.
166 2017) and it has been shown that base-pairing of TC with nucleotides upstream to the BPS
167 can help to stabilize U2-BPS interaction (Xu and Query 2007). Scores were determined as
168 described in Materials and Methods section taking into account that, as described for minor
169 BPS, either of two adjacent adenosines within the branch site sequence can be used as the
170 branchpoint nucleotide (Query et al. 1994). Results presented in Table 1 indicate that the
171 highest U2 scores (16 and 14) correspond to branchpoint sequences represented in several
172 minor introns such as Tsta3, Llglh and Gosr1 (Figure 5B and C), whose retention is not
173 significantly affected in SMA spinal cords, despite of moderate U12 scores (<17). For lower
174 U2 scores, splicing of the corresponding introns (such as Vac14, Exosc1, Ncoa6ip and Ints7)
175 is significantly inhibited (Table 1; Figure 4 and 5).

176 Altogether, these observations reinforce the hypothesis that splicing of a subset of
177 minor introns can depend on both the minor and major spliceosome activities.

178

179 **In vitro splicing of the Tsta3 minor intron depends on both minor and major** 180 **spliceosomes components.**

181 In order to evaluate the role of the major spliceosome in the splicing of minor introns,
182 we constructed four reporters sharing similar splice donors, splice acceptors and intron sizes
183 but differing at the level of their branchpoint sequence (Figure 6). In the Slc12a4 construct,
184 the BPS corresponds to the consensus sequence and exhibit the highest U12 score (U12=19)
185 but an intermediate U2 score (U2=9). This intron belongs to the category whose splicing is

186 only slightly affected in SMA spinal cords (Table 1; Figure 3A and 3C). The Tsta3 reporter
187 contains a minor intron with a poor U12 BPS (U12 score=14) which in turn exhibits a high
188 U2 score (U2=16). As shown in Figure 5B and 5C, splicing of this intron is not inhibited, and
189 even moderately increased, in SMN-deficient spinal cords. The third construct, Hip1r,
190 contains a minor intron whose BPS exhibits a medium score for U12 (U12=15) and a good
191 enough U2 score (U2=15). The last reporter, Vac14, contains a minor intron with a BPS
192 whose score is very low for both U12 and U2 (U12=12 and U2=4). As a consequence,
193 splicing of this intron is significantly inhibited in SMA spinal cord (Figure 4B and 4C).

194 *In vitro* splicing experiments were performed with the different reporters in HeLa
195 nuclear extracts and splicing products were analyzed as described in Materials and Methods.
196 To test whether splicing only depends on the minor spliceosome or also involves the major
197 splicing machinery, nuclear extracts were pre-incubated with locked nucleic acids (LNAs)
198 targeting the U12 or U2 snRNAs. As expected, treatment of nuclear extracts with U12 LNA
199 had a significant effect on Slc12a4, Tsta3, Hip1r and Vac14 splicing efficiency (2.0, 2.5, 4.0
200 and 8.0 fold decrease, respectively; Figure 7A and B). A much lower reduction of the splicing
201 efficiency was observed for the Slc12a4, Tsta3, Hip1r and Vac14 reporters following pre-
202 incubation of the nuclear extracts with the U2 LNA (1.3, 1.4, 2.1 and 1.15 fold decrease,
203 respectively, statistically non-significant). Interestingly, simultaneous treatment with the U12
204 and U2 LNAs had no effect on the Slc12a4 splicing efficiency as compared to that observed
205 following U12 LNA treatment alone, whereas splicing of the Tsta3 reporter was further
206 decreased by 4.0 fold under the same conditions. For the Hip1r reporter whose BPS U2 score
207 is slightly lower than that of the Tsta3 intron, splicing efficiency observed upon U12
208 inactivation was also reduced by 2.0 fold (non significant) following treatment with U12 and
209 U2 LNAs. In the same conditions, splicing of the Vac14 reporter was reduced by 75%,
210 although in a non-significant way, as compared to the U12 inhibition alone. These
211 observations indicate that splicing of the Tsta3 minor intron is significantly affected by U12
212 inactivation and even more when both U2 and U12 are targeted, thereby suggesting that
213 components of the major spliceosome likely play a substantial role in its splicing.

214 To determine whether the major spliceosome can, on its own, carry out splicing of the
215 Tsta3 minor intron, *in vitro* splicing experiments were performed following treatment of the
216 nuclear extracts with a much higher concentration of U12 LNA. Under these conditions,
217 splicing of the Slc12a4 reporter is almost no longer detectable (Figure 7C and D) while that of
218 the Tsta3 minor intron is fully inhibited, thereby indicating that the major splicing machinery
219 alone is not able to achieve removal of this intron. Moreover, these observations strongly
220 suggest that a sufficient amount of functional U12 snRNP is required to allow the
221 involvement of the U2 snRNP in this process.

222

223 **The Plcb3 minor intron contains competing BPSs differentially affected by U2 depletion.**

224 To exclude the possibility that the effect of U2 depletion is specific for the Tsta3
225 splicing reporter, we performed similar *in vitro* splicing experiments with the Plcb3 construct
226 (Figure 8A) in which the BPS (CTGACCGAC) has a high U2 score (U2=15). Surprisingly, *in vitro*
227 splicing of this construct gives rise to the expected product (245nt) but also to a shorter
228 one (127nt) not already described (Figure 8B). Sequencing of this product indicated that it
229 results from the use of an alternative 3' splice site located 7 nt upstream from the end of the 3'

230 exon. Careful examination of the intronic sequence allowed us to identify a potential BPS
231 (GCCCTCAAC) where the branchpoint adenosine is located 8 nt upstream from the
232 alternative 3' splice site and whose U12 and U2 scores are low (U12=13; U2=10).
233 Interestingly, treatment of the nuclear extracts with the U12 LNA resulted in a significant
234 decrease of both the expected and the alternative splicing products (3.2 and 4.9 fold decrease,
235 respectively), whereas treatment with the U2 LNA only affected the splicing efficiency of the
236 expected splicing product (2.4 fold decrease; Figure 8C). Following simultaneous treatment
237 with the U12 and U2 LNAs, the splicing efficiency of the expected and alternative products
238 was further reduced by 4 fold and 3.2 fold, although in a statistically non-significant way, as
239 compared to the U12 inhibition alone (Figure 8C). Taken together, these observations indicate
240 that the splicing efficiencies of the two Plcb3 products are differentially affected by U2
241 depletion, in good agreement with the U2 score of their corresponding branchpoint sequence.

242

243 **The branchpoint sequence is responsible for the U2 snRNP-dependent splicing of Tsta3** 244 **minor intron.**

245 To definitely establish that the sequence of the BPS is responsible for the involvement
246 of major spliceosome components in the splicing of the Tsta3 minor intron, we performed
247 swapping experiments to replace its original BPS by that of the Slc12a4 intron. As shown in
248 Figure 9, the splicing efficiency of the Tsta3 BPS Slc12a4 construct is increased as compared
249 to that of the original Tsta3 reporter and very similar to that of the Slc12a4 reporter (Figures 7
250 and 9). Upon treatment of the nuclear extracts with the U12 LNA, the splicing efficiency was
251 reduced by 1.85 fold, this decrease being consistent with that observed for the original
252 Slc12a4 reporter (Figures 7 and 9). Noteworthy, an alternative product was detected in these
253 conditions, indicative of the activation of cryptic splice sites. Sequencing of this product
254 indeed revealed that major donor (TG/GTGAGG) and acceptor (CAAG/GC) sites located
255 within the Tsta3 intron are used to generate this variant RNA (Figure 9B). Following
256 treatment with the U2 LNA, the alternative product was no longer detected, thereby
257 confirming that its results from the activity of the major spliceosome (Figure 9A and 9C).
258 Under the same conditions, the minor splicing efficiency was slightly reduced (1.4 fold),
259 although in a non-significative way, as already observed for the Slc12a4 construct (Figures 7
260 and 9). Simultaneous treatment with the U12 and U2 LNAs had no significant effect on the
261 Tsta3 BPS Slc12a4 splicing efficiency as compared to that observed following U12 LNA
262 treatment alone (Figure 9A and 9C). These observations indicate that the Slc12a4 BPS is
263 sufficient, per se, to confer to the Tsta3 construct the splicing behavior of the Slc12a4 reporter
264 and to abrogate its dependency toward the U2 snRNA.

265 Interestingly, the splicing behavior of the Tsta3 construct was restored following
266 replacement of the Slc12a4 BPS by that of the Mapk1 minor introns which exhibit a
267 suboptimal U12 score (15; Table 1) but a rather high U2 score (14; Table 1), and whose
268 splicing is not affected in SMA spinal cords (Figure 2). Indeed, U12 and U2 degradation led
269 to a ~1.4 and ~1.5 fold decrease of the splicing efficiency, respectively. Following
270 simultaneous U12 and U2 LNA treatment, the splicing efficiency of the Tsta3 BPS Mapk1
271 reporter was decreased by 5.0 fold as compared to the U12 LNA treatment alone (Figure 9A
272 and 9D). As already observed for the Tsta3 construct (Figure 7C and 7D), splicing of the
273 Tsta3 BPS Mapk1 reporter was fully inhibited following treatment of the nuclear extracts

274 with a high U12 LNA concentration (Figure 9E and 9F), confirming that a sufficient amount
275 of functional U12 snRNP is required to allow the involvement of the U2 snRNP in their
276 splicing.

277 Altogether, these results indicate that the U2 snRNP from the major spliceosome can
278 contribute to the splicing of minor introns, in a way that is mainly dependent on their
279 branchpoint sequence.

280

281 **U2 snRNAs interact with the Tsta3 BPS.**

282 To determine whether the U2 snRNA interacts with the Tsta3 BPS, we performed UV
283 cross-linking experiments with the Tsta3 reporter as well as with the Tsta3 BPS Slc12a4
284 construct where the original Tsta3 BPS has been exchanged for that of the Slc12a4 reporter
285 (Figures 7 and 9). In vitro splicing reactions were performed in the presence of the splicing
286 inhibitor Isoginkgetin (O'Brien et al. 2008) which prevents the stable recruitment of the
287 U4/U5/U6 and U4atac/U5/U6atac tri-snRNPs and results in the accumulation of the
288 prespliceosomal A complexes. Following UV crosslinking, RNA was purified, hybridized to
289 biotinylated oligonucleotides specific for Tsta3 intronic and 3' exon sequences, and reporter
290 pre-mRNAs were affinity-purified with Streptavidin-coupled magnetic beads. Amounts of
291 U12 and U2 snRNAs copurifying with the reporter pre-mRNAs were determined by RT-PCR
292 analyses using primers located in the 3' region of both snRNAs in order to avoid strong
293 reverse transcriptase stops induced by UV irradiation. Indeed, using UV-crosslinking of
294 purified U2 snRNPs, Dybkov et al. (2006) reported that only five faint UV-dependent reverse
295 transcriptase stops (A123, C128, U130, G131 and C135) occur in the region comprised
296 between nucleotides 104 and 149 of the U2 snRNA, whereas much stronger UV-dependent
297 stops are observed upstream. In good agreement with this study, we were able to amplify U2
298 sequences with oligonucleotides located at positions 105-125 (Fw) and 157-176 (Rev;
299 Figure10) but not with an upstream forward primer located at positions 65-84 (Data not
300 shown). To detect U12 sequences, we tested two primer pairs (Fw: 39-58 x Rev: 124-145 and
301 Fw: 81-101 x Rev: 124-145) and we found that both allowed efficient amplification (Figure
302 10 and data not shown).

303 As controls, we analyzed the amounts of snRNAs copurified with magnetic beads
304 alone (without reporter RNAs) or with reporter RNAs without crosslinking. As shown in
305 Figure 10, the amount of U12 snRNA copurified with the beads alone was nearly
306 undetectable whereas U2 snRNAs were significantly detected, thereby indicating non specific
307 sticking proportional to the relative amounts of these two snRNAs in the splicing extracts.
308 When reporter RNAs were incubated in the splicing extracts but not submitted to UV
309 crosslink, the amounts of copurified snRNAs were not significantly different than those
310 obtained with the beads alone. After UV crosslink, the amount of U12 snRNA was only
311 slightly increased for both reporters, consistent with the low abundance of minor snRNAs
312 (Montzka and Steitz 1988) and likely because of the short incubation time we used prior to
313 UV irradiation. Strikingly, the amount of U2 snRNAs was increased by ~1.7 fold for the
314 Tsta3 reporter as compared to that obtained with the beads alone or when crosslinking is
315 omitted, whereas that obtained with the Tsta3 BPS Slc12a4 construct was not changed. To
316 confirm the U2 snRNA enrichment observed with the Tsta3 reporter, we performed semi-
317 quantitative RT-PCR analyses as described in the Materials and Methods section. As shown

318 in Figure 10 C and D, amplification of the products corresponding to U2 snRNA and Tsta3
319 exon 2 used for normalization increased up to 24 cycles, indicating that the reaction is still in
320 its exponential range. Quantification of the signals obtained after 18 cycles for two
321 independent experiments indicated that the amount of U2 snRNA obtained with the Tsta3
322 reporter is increased by ~1.8 fold as compared to that detected with the Tsta3 BPS Slc12a4
323 construct (Figure 10E).

324 Altogether, these observations confirm that the Tsta3 branchpoint sequence efficiently
325 interacts with the U2 snRNA.

326

327 **The Tsta3 branchpoint sequence increases the rate of the splicing reaction.**

328 In order to determine whether the Tsta3 BPS-U2 snRNA interaction increases the
329 splicing rate of high U2 score reporters, we performed time course analyses of the splicing
330 reaction using radiolabeled Tsta3 and Tsta3 BPS Slc12a4 transcripts. As shown in Figure
331 11A, products of the first step of the splicing reaction, lariat-exon 2 and exon 1 (visible after
332 long exposure) were detected for both reporters following 5 minutes of incubation. Strikingly,
333 spliced RNA was also clearly detected after 10 and 15 minutes for the Tsta3 reporter whereas
334 it was still barely visible after 20 minutes for the Tsta3 BPS Slc12a4 transcript. Analysis of
335 the splicing efficiencies (Figure 11B) confirmed that the splicing reaction proceeds faster for
336 the Tsta3 substrate than for the Tsta3 BPS Slc12a4 transcript (Between 4.5 fold after 5
337 minutes and 2 fold after 20 minutes of incubation). In a longer time course study (20 to 100
338 minutes), we observed the apparition of the lariat product, at the expense of the lariat-exon 2
339 intermediate, as well as the accumulation of the spliced RNA. From 20 to 100 minutes, the
340 splicing efficiency of the Tsta3 substrate was always higher (between 2.2 and 1.4 fold) than
341 that of the Tsta3 BPS Slc12a4 transcript (Figure 11A and 11C).

342 Taken together, these results indicate that interaction of the Tsta3 BPS with the U2
343 snRNP correlates with increased splicing rate and efficiency as compared with those observed
344 for the Tsta3 BPS Slc12a4 substrate, yet containing an optimal U12 branchpoint sequence.

345 **DISCUSSION**

346 Splicing inhibition of U12-dependent introns has been reported in SMA patient cells
347 (Boulisfane et al. 2011) as well as in a severe SMA mouse model (Zhang et al; 2008; Doktor
348 et al. 2017; Jangi et al. 2017). Among all introns whose retention is increased in the SMA
349 mice, minor introns are preferentially affected and nearly one third of them exhibit significant
350 retention levels (Doktor et al. 2017). Aside from its role in driving the assembly of major
351 spliceosomal snRNPs, SMN is also involved in the biogenesis of minor snRNPs (Zhang et al.
352 2008) which are much less abundant than their major counterparts (Montzka and Steitz 1988).
353 This, along with the observation that splicing of minor introns is already a slow process under
354 physiological conditions (Patel et al. 2002; Pessa et al. 2006), could explain why minor
355 splicing is preferentially impacted by SMN depletion.

356 Our previous studies allowed us to show that splicing of some, but not all, minor
357 introns is significantly affected in SMA patient lymphoblasts (Boulisfane et al. 2011). In the
358 present study, we have investigated the molecular bases of this differential intron retention by
359 analyzing the splicing efficiency of ~ 30 minor introns in spinal cords of a mild SMA mouse
360 model. Our results indicate that the very stringent and highly conserved branchpoint sequence
361 of the minor introns is the primary determinant of this process. Indeed, we show that splicing
362 of minor introns containing consensus branchpoint sequences is not significantly affected,
363 whereas that of most introns with suboptimal BPS (U12 score <17) is inhibited in spinal cords
364 of SMA mice (Figures 3 and 4). Interestingly, we identified minor introns harboring non
365 consensus BPSs and whose splicing is nevertheless not affected in SMA mice (Figure 5).
366 Since these suboptimal BPSs exhibit an increased capacity to interact with the anti-branch site
367 of the U2 snRNA, this led us to test whether components of the major spliceosome could play
368 a role in the processing of these minor introns. Using *in vitro* splicing experiments and LNAs
369 targeting U12 and/or U2 snRNAs, we have shown for the first time that splicing of a subset of
370 minor introns depends on both splicing machineries. To date, the sole example of an intron
371 whose splicing relies on components of the two spliceosomes is a major intron of the Rat
372 CGRP gene (Roesser 2004). The context is however different because splicing of CGRP exon
373 5, which is dependent on the major spliceosome, also requires the U12 snRNP but the exact
374 role of this minor splicing component has not been elucidated.

375 Our *in vitro* splicing experiments performed with reporters containing branchpoint
376 sequences with different U2 scores strongly suggested that involvement of the U2 snRNP in
377 the splicing of several minor introns proceeds through direct binding of the U2 snRNA to the
378 branchpoint motif. This has been further confirmed by *in vitro* splicing assays performed with
379 Tsta3 reporters only differing by their branchpoint sequence (Figure 9) and by cross-linking
380 experiments (Figure 10) showing that the Tsta3 reporter containing its genuine BPS
381 (GGTCTTGAC ; U2 score=16) efficiently binds U2 snRNAs whereas the same construct
382 containing the Slc12a4 BPS (TTCCTTAAC ; U2 score=9) does not. Finally, time course
383 analyses of splicing reactions performed with these two reporters have revealed that
384 involvement of the U2 snRNP in the splicing of the Tsta3 substrate results in an increased rate
385 and a better efficiency of intron excision as compared to those observed for the Tsta3 BPS
386 Slc12a4 (Figure 11)

387 In major introns, interaction between the U2 snRNP and the branchpoint sequence
388 requires prior binding of the U2 auxiliary factor (U2AF) to the polypyrimidine tract (PPT)

389 located downstream of the BPS (Ruskin et al. 1988; Michaud and Reed 1991; 1993). Since
390 minor introns lack apparent PPTs between the BPS and the 3' splice site (Sharp and Burge
391 1997), this raises the question to know how the interaction of the U2 snRNP with specific
392 minor BPSs can be promoted and/or stabilized. A likely explanation relies on the exon-
393 definition model initially reported for splicing of major introns and whereby U1 snRNP
394 bound to a 5' splice site can be bridged to the U2AF complex bound to an upstream PPT
395 through interactions with Arginine-Serine-rich (SR) proteins (Robberson et al. 1990; Hoffman
396 and Grabovsky 1992; Wu and Maniatis 1993). Later on, it was shown that such a model can
397 also apply to minor intron splicing since addition of a major 5' splice downstream of a minor
398 splicing reporter enhances the excision of the upstream minor intron (Wu and Krainer 1996).
399 In that situation, bridging between U1 and U12 snRNPs would then occur through
400 interactions with SR proteins and maybe other factors likely related to U2AF proteins such as
401 Zrsr2/Urp (Shen et al. 2010) compensating for the absence of U2AF (Figure 12).

402 Our *in vitro* studies also reveal that the almost complete inactivation of the U12
403 snRNP results in the full splicing inhibition of the Tsta3 minor intron (Figure 7C and D),
404 thereby indicating that the major spliceosome is not, by itself, able to carry out the removal of
405 this intron. This is consistent with the fact that consensus minor 5' splice sites (such as that of
406 the Tsta3 intron i.e. GTATCCTTT) do not contain a G at position +5 which is involved in a
407 crucial base-pairing interaction with the U6 snRNA (Kandel Lewis and Seraphin 1993; Lesser
408 and Guthrie 1993). Moreover, the nucleotide at position -1 in minor 5' splice sites of the GT-
409 AG subtype is generally a U (Moyer et al. 2020), whereas a G is preferred in major 5' splice
410 sites because it pairs with a C in the U1 snRNA (Pomeranz Krummel et al. 2009; Kondo et al.
411 2015). Altogether, these observations argue against a role of the U1 snRNP in the splicing of
412 the Tsta3 intron but rather support a cooperation between the minor U11-U12 di-snRNP and
413 the U2 snRNP in the pre-spliceosomal A complex. Our results also raise interesting questions
414 concerning the need for functional U12 snRNPs to reveal the role of the U2 snRNP in the
415 splicing of the Tsta3 minor intron. It has been shown that all the U12 snRNPs exist as di-
416 snRNP complexes in splicing extracts (Montzka and Steitz 1988; Wassarman and Steitz 1992)
417 and that treatment of nuclear extracts with a U12-specific 2'-O-methyl oligonucleotides
418 results in a dramatic decrease of U11 snRNP binding to the 5' splice site of a P120 minor
419 splicing substrate (Frilander and Steitz 1999). One can therefore envisage that complete
420 inactivation of the U12 snRNP precludes binding of the di-snRNP to the 5' splice site or that
421 structural modifications of the inactivated U12 snRNP inhibit the formation of the chimeric
422 spliceosomal A complex. Along this line, formation of this complex could involve
423 interactions between the U2 and U12 snRNPs, either in a direct way or through binding to an
424 additional factor which remains to be identified (see below; Figure 12A). In an alternative
425 model, interactions could be established between the U2 and U11 snRNPs (Figure 12B). In
426 support of the latter model, a recent study suggests that the U11-59K protein of the minor
427 spliceosome could bind proteins of the major spliceosome to form exon-bridging interactions
428 involved in the regulation of alternative splicing events around minor introns (Olthof et al.
429 2021). Strikingly, one of the proteins bound by U11-59K is SF3B1 (SF3b155) which is part
430 of the U2 snRNP (Reed 1996). These observations would therefore confirm previous reports
431 indicating the existence of crosstalks between the two splicing machineries (Wu and Krainer
432 1996; Cologne et al. 2019; Akinyi and Frilander 2021).

433 The involvement of the U2 snRNP in the splicing of several minor introns raises
434 interesting questions concerning the evolutionary fate of these introns. Indeed, the high U2
435 score exhibited by their BPS suggest that this subset of minor introns could correspond to
436 those undergoing U12- to U2-type conversion. Evolutionary mechanisms concerning minor
437 introns have been documented twenty years ago (Burge et al. 1998) and it was proposed that
438 the conversion from the U12 to the U2 splicing type first requires mutation of the highly
439 conserved U12 5' splice site (GTATCCTTT), generally at the +5 position, to be recognized
440 by the U1 snRNP. It was also suggested that the C/T-rich minor BPS (TTCCTTRAY) could
441 fulfil the role of the pyrimidine-rich region important in the splicing of U2 introns, and that an
442 upstream motif close to the highly degenerated U2 BPS could be used as a functional major
443 branch site. The situation described in our study is somewhat different because we identified
444 minor introns which contain suboptimal U12 BPS and exhibit an increased capacity to
445 interact with the U2 snRNA. Our analyses thereby support another model where the U12 BPS
446 can be recognized by either the U12 or U2 snRNA. In the latter case, the absence of a PPT
447 suggest that the U2AF complex, known to help anchoring U2 snRNP at the BPS, is not
448 involved in the recognition of the 3' splice site. However, it has been shown that for major
449 introns with weak PPTs, interaction of the U2AF35 subunit with the 3' splice site
450 dinucleotide AG is determinant for U2AF binding and splicing (Merendino et al. 1999; Wu et
451 al. 1999; Zorio and Blumenthal 1999). Alternatively, U2AF could be replaced by a U2AF-
452 related protein such as ZRSR2/Urp (Figure 11) which is not only required for minor introns
453 splicing but also for the second step of major introns splicing where it is thought to replace
454 U2AF35 (Shen et al. 2010).

455 Overall, our study is revealing the existence of a cooperative crosstalk between
456 components of both the minor and major splicing machineries participating to the efficient
457 splicing of a subset of minor introns containing suboptimal BPSs. The ability of the
458 branchpoint sequence to interact with the U2 snRNA could help to preserve efficient splicing
459 of the corresponding minor introns, not only upon SMN depletion, but also in other diseases
460 such as Isolated Growth Hormone Deficiency (IGHD) and Cerebellar Ataxia (Reviewed in
461 Verma et al. 2018) which result from mutations of minor spliceosome components affecting
462 the intron recognition step.

463

464 **MATERIALS AND METHODS**

465

466 **Animals**

467 SMN Δ 7 founder mice were purchased from Jackson (stock number: 5025). These mice harbor
468 a single targeted mutation (disruption of exon 2 in the endogenous mouse *Smn* gene and two
469 transgenic alleles, the entire human *SMN2* gene and a *SMN1* cDNA lacking exon 7 (*SMN Δ 7*).
470 Wild-type mice were [*SMN2*^{+/+}, *SMNdelta7*^{+/+}, *Smn*^{+/+}], heterozygous mice were [*SMN2*^{+/+},
471 *SMNdelta7*^{+/+}, *Smn*^{+/-}] and SMNdelta7 mice were [*SMN2*^{+/+}, *SMNdelta7*^{+/+}, *Smn*^{-/-}]. The
472 clinical signs are apparent at 5 days, and mean survival is approximately 13 days.
473 Heterozygous breeding pairs were mated and litters were genotyped at birth. Mice were kept
474 under controlled conditions (22 \pm 1°C, 60 \pm 10% relative humidity, 12-hour light 12-hour dark
475 cycle, food and water *ad libitum*). Care and manipulation of mice were performed in
476 accordance with national and European legislations on animal experimentation and approved
477 by the institutional ethical committee.

478

479 **Tissue sampling**

480 Spinal cords were collected 12-13 days after birth. Mice were deeply anesthetized by
481 intraperitoneal injection of 100 mg/kg ketamine 1000 (Imalgène 1000, 100 mg/ml, Merial,
482 France) and 10 mg/kg xylazine (2 %, Rompun, Bayer, France) and intracardially perfused
483 with phosphate buffer solution (PBS). The spinal cord was harvested and immediately flash-
484 frozen in liquid nitrogen for total RNA purification.

485

486 **Total RNA purification and RT-PCR analyses**

487 Total RNA was purified from spinal cords with Tri-Reagent (Sigma) according to the
488 manufacturer's procedure and treated with RQ1 DNase (1 unit per μ g; Promega) for 40 min at
489 37°C. First-strand cDNA was synthesized from 5 μ g of total RNA and pd(N)6 random
490 oligonucleotides with First strand cDNA synthesis kit (Cytiva/GE-Healthcare). For PCR
491 analyses, the RT reaction was diluted to obtain a 40 ng/ μ l concentration of starting RNA
492 material. Primers were designed so as to amplify simultaneously the unspliced (Exon_n forward
493 x Intron_n reverse) and spliced forms (Exon_n forward x Exon_{n+1} reverse) in the same PCR
494 reaction. For short introns (<250 nt), only the Exon_n forward and Exon_{n+1} reverse primers
495 were used.

496 Three μ l of the diluted RT reaction were amplified with GoTaq polymerase (Promega) in a
497 volume of 50 μ l containing 20 pmoles of each of the 3 primers, 200 μ M dNTPs and 1.5 mM
498 MgCl₂ in 1x GoTaq buffer; Reactions were cycled 25-30 times, depending of the mRNA
499 expression level. For very weakly expressed mRNAs, reactions were cycled up to 40 times.
500 Primer sequences and PCR regimes are available on request. The PCR products were
501 separated on 1.5-2.0 % agarose gels containing ethidium bromide and visualized under UV
502 light. The gel images were digitally captured and analyzed using ImageJ software. Intron
503 retention was calculated by dividing the signal of the unspliced form by the total (spliced +
504 unspliced) signal.

505

506

507 **Construction of splicing reporters**

508 Splicing reporters were amplified from mouse genomic DNA (Slc12a4, Plcb3) or cDNA
509 (Tsta3, Hip1r). In order to maintain a similar intron size in all the reporters, the Vac14
510 reporter was constructed by PCR recombination of 2 fragments lacking the central part of the
511 original intron. In all constructs, the downstream major splice site was included because it has
512 been reported that this improves the *in vitro* splicing efficiency (Wu and Krainer 1996). The
513 different reporters were introduced into the PGEM-9Z plasmid (Promega) and sequence-
514 verified. Following linearization of the reporters, *in vitro* transcription was performed with T7
515 RNA polymerase according to the manufacturer's instructions.

516 BPS swapping experiments were performed by PCR mutagenesis with oligonucleotides
517 overlapping the Tsta3 sequences and containing either the Slc12a4 (TTCCTTAAC) or the
518 Mapk1 (GACCTTAAC) branchpoint motif.

519

520 ***In vitro* splicing experiments and RT-PCR analyses**

521 Transcripts were synthesized *in vitro* for 2 hours at 37°C with 40 units of T7 RNA
522 polymerase (NEB) in the presence of 500 µM ATP, CTP, UTP, 200 µMGTP, 1.25 mM Cap
523 analog, 10 mM DTT, 30 units of RNasin and 1.5 µg of linearized DNA template in the
524 recommended transcription buffer. Following RQ1 DNase treatment, reactions were extracted
525 with phenol-chloroform and precipitated overnight at -20°C.

526 *In vitro* splicing experiments were performed 5 hours at 34° C in a 40 µl mix containing 60%
527 HeLa nuclear extracts (Ipratech), 2,4 mM MgCl₂, 2,5 mM ATP, 20 mM phosphocreatine
528 (Sigma), 10 units creatine kinase (Sigma), 1 % polyvinyl alcohol and 10 ng of purified
529 transcript.

530 For inactivation of major or minor snRNPs, reaction mixtures were pre-incubated 20 minutes
531 at 34° C in the presence of corresponding Locked Nucleic Acids (LNA) before addition of the
532 splicing substrates. LNA U2 (27-49; Lamond et al. 1989; Tarn and Steitz 1996):
533 ATAAGAACAGATACTACACTTGA; LNA U12 (11-28; Tarn and Steitz 1996):
534 ATTTTCCTTACTCATAAG (underlined nucleotides indicate modified bases).

535 Following proteinase K digestion for 30 minutes at 37°C, RNA species were phenol-extracted
536 and precipitated with ethanol in the presence of 1.5 µg glycogen. Unspliced and spliced
537 products were reverse transcribed with First strand cDNA synthesis kit (Cytiva/GE-
538 Healthcare) using 33 pmoles of reverse primers specific for each construct. For RT-PCR
539 analyses, the RT reaction was diluted to obtain a 0.66 ng/µl concentration of starting RNA
540 transcript. Three µl of RT reaction were amplified for 30 cycles with primers located in the
541 upstream and downstream exons of each splicing reporter. Splicing efficiency was calculated
542 by dividing the signal of the spliced form by the total (spliced + unspliced) signal.

543

544

545 **UV-Cross Linking experiments**

546 *In vitro* splicing reactions were assembled as described above in a final volume of 200 µl
547 containing 75 ng of purified transcripts and in the presence of 70 µM Isoginkgetin

548 (MedChemExpress). Following a 45 min incubation at 34°C, reaction mixtures were diluted
549 ten fold in buffer E (12 mM HEPES-NaOH pH 7.9, 60 mM KCl, 1.5 mM MgCl₂, 0.12 mM
550 EDTA, 12% glycerol) to minimize nonspecific cross-linking and irradiated two times with
551 UV light (wavelength 254 nm) in Stratalinker (Stratagene) at 250,000 μJ/cm² on a 6-well
552 culture plate on ice at a distance of 10 cm from UV light. Control experiments without
553 reporter RNAs (Control Beads) or where the UV crosslinking step was omitted were also
554 performed. Following proteinase K digestion for 30 minutes at 37°C, RNAs were phenol-
555 extracted and precipitated with ethanol in the presence of 1.5 μg glycogen. RNAs were
556 resuspended in 200 μl of Dignam's buffer D (Dignam et al. 1983) and hybridized to two 5'-
557 biotinylated oligonucleotides (10 pmoles each) specific for Tsta3 intron and 3' exon
558 sequences by heating at 70°C for 5 min and slow cooling at room temperature. Hybridized
559 RNAs were captured with 150 μg MyOne™ Streptavidin C1 Dynabeads (Invitrogen), washed
560 three times with 200 μl of 1X BW buffer (5 mM Tris-HCl pH 7.5, 0.5 mM EDTA, 1 M NaCl)
561 and eluted at 70°C for 5 min in 30 μl of RNase-free water.

562 First-strand cDNA was synthesized from 5 μl of eluted RNA and pd(N)6 random
563 oligonucleotides with First strand cDNA synthesis kit (Cytiva/GE-Healthcare). For PCR
564 analyses, one fifth of the RT reaction was amplified with primers pairs specific for U12 (Fw:
565 5'GGTGACGCCCGAATCCTCAC3'; Rev: 5'AGATCGCAACTCCCAGGCATCC3') or U2
566 (Fw: 5'GGAGCAGGGAGATGGAATAGG3'; Rev: 5'CCTGGAGGTACTGCAATACC3')
567 snRNAs as well as for Tsta3 3' exon (E2, Fw: 5'TTTGATTCAACAAAGTCAGATGGG3' ;
568 Rev : 5'GAAGGGTGTGAAACGGAAGTC3') for normalization. The gel images were
569 digitally captured and analyzed using ImageQuant TL software.

570 For semi-quantitative RT-PCR analyses, cDNA was amplified as mentioned above in the
571 presence of 2 μCi dCTP α-³²P (Hartmann Analytics; 3000 Ci/mmol.) and the concentration of
572 the corresponding nucleotide was lowered to 40 μM. One fifth of the PCR products was
573 separated in a 10% non-denaturing polyacrylamide gel and visualized by autoradiography at -
574 80°C. The gel images were digitally captured and analyzed using ImageJ software.

575

576 **Time course analyses of splicing reactions**

577 Radiolabeled transcripts were synthesized as described above in the presence of 60 μCi UTP
578 α-³²P (Hartmann Analytics; 800 Ci/mmol.) and the concentration of the corresponding
579 nucleotide was lowered to 50 μM. Transcripts were gel-purified and 50 000 cpm were used
580 for the splicing reactions. Reactions were stopped at the indicated times by quick freezing in
581 dry ice. Following proteinase K digestion, splicing products were extracted with phenol-
582 chloroform, precipitated overnight at -20°C and separated in 4% and 6% denaturing (8M
583 Urea) polyacrylamide gels. After autoradiography at -80°C, gel images were digitally
584 captured and analyzed using ImageJ software. Signals corresponding to spliced and unspliced
585 species were normalized according to their uridine content. Splicing efficiency was calculated
586 by dividing the signal of the spliced form by the spliced + unspliced signal.

587

588

589

590 **FUNDING**

591 This study was supported by the CNRS and by a grant of the Association Française contre les
592 Myopathies (N°17760) to J.S.

593 **ACKNOWLEDGEMENTS**

594 We thank Drs. F. Rage and T. Forné for critical reading of the manuscript and helpful
595 discussions. The authors declare that they have no conflict of interest.

596

597

598 **REFERENCES**

599

- 600 Akinyi MV, Frilander MJ. 2021. At the Intersection of Major and Minor Spliceosomes:
601 Crosstalk Mechanisms and Their Impact on Gene Expression. *Front Genet* **12**:700744.
- 602 Alioto TS. 2007. U12DB: a database of orthologous U12-type spliceosomal introns. *Nucleic
603 Acids Res* **35**: D110-115.
- 604 Boulisfane N, Choleza M, Rage F, Neel H, Soret J, Bordonné R. 2011. Impaired minor tri-
605 snRNP assembly generates differential splicing defects of U12-type introns in lymphoblasts
606 derived from a type I SMA patient. *Hum Mol Genet* **20**: 641–648.
- 607 Brock JE, Dietrich RC, Padgett RA. 2008. Mutational analysis of the U12-dependent branch site
608 consensus sequence. *RNA* **14**: 2430–2439.
- 609 Burge CB, Padgett RA, Sharp PA. 1998. Evolutionary fates and origins of U12-type introns. *Mol
610 Cell* **2**: 773–785.
- 611 Burnett BG, Muñoz E, Tandon A, Kwon DY, Sumner CJ, Fischbeck KH. 2009. Regulation of
612 SMN protein stability. *Mol Cell Biol* **29**: 1107–1115.
- 613 Champion Y, Neel H, Gostan T, Soret J, Bordonné R. 2010. Specific splicing defects in *S. pombe*
614 carrying a degron allele of the Survival of Motor Neuron gene. *EMBO J* **29**: 1817–1829.
- 615 Cartegni L, Krainer AR. 2002. Disruption of an SF2/ASF-dependent exonic splicing enhancer in
616 SMN2 causes spinal muscular atrophy in the absence of SMN1. *Nat Genet* **30**: 377–384.
- 617 Charroux B, Pellizzoni L, Perkinson RA, Yong J, Shevchenko A, Mann M, Dreyfuss G. 2000.
618 Gemin4. A novel component of the SMN complex that is found in both gems and nucleoli. *J
619 Cell Biol* **148**: 1177–1186.
- 620 Cho S, Dreyfuss G. 2010. A degron created by SMN2 exon 7 skipping is a principal contributor
621 to spinal muscular atrophy severity. *Genes Dev* **24**: 438–442.
- 622 Cologne A, Benoit-Pilven C, Besson A, Putoux A, Campan-Fournier A, Bober MB, De Die-
623 Smulders CEM, Paulussen ADC, Pinson L, Toutain A, Roifman CM, Leutenegger AL,
624 Mazoyer S, Edery P, Lacroix V. 2019. New insights into minor splicing-a transcriptomic
625 analysis of cells derived from TALS patients. *RNA* **25**:1130-1149.
- 626 Coover DD, Le TT, McAndrew PE, Strasswimmer J, Crawford TO, Mendell JR, Coulson SE,
627 Androphy EJ, Prior TW, Burghes AH. 1997. The survival motor neuron protein in spinal
628 muscular atrophy. *Hum Mol Genet* **6**: 1205–1214.

629 Crawford TO, Pardo CA. 1996. The neurobiology of childhood spinal muscular atrophy.
630 *Neurobiol Dis* **3**: 97–110.

631 Custer SK, Gilson TD, Li H, Todd AG, Astroski JW, Lin H, Liu Y, Androphy EJ. 2016. Altered
632 mRNA Splicing in SMN-Depleted Motor Neuron-Like Cells. *PLoS ONE* **11**: e0163954.

633 Dietrich RC, Inorvaia R, Padgett RA. 1997. Terminal intron dinucleotide sequences do not
634 distinguish between U2- and U12-dependent introns. *Mol Cell* **1**: 151–160.

635 Dignam JD, Lebowitz RM, Roeder RG. 1983. Accurate transcription initiation by RNA
636 polymerase II in a soluble extract from isolated mammalian nuclei. *Nucleic Acids Res* **11** :
637 1475-1489.

638 Doktor TK, Hua Y, Andersen HS, Brøner S, Liu YH, Wieckowska A, Dembic M, Bruun GH,
639 Krainer AR, Andresen BS. 2017. RNA-sequencing of a mouse-model of spinal muscular
640 atrophy reveals tissue-wide changes in splicing of U12-dependent introns. *Nucleic Acids Res*
641 **45**: 395–416.

642 Dybkov O, Will CL, Deckert J, Behzadnia N, Hartmuth K, Lührmann R. 2006. U2 snRNA-
643 protein contacts in purified human 17S U2 snRNPs and in spliceosomal A and B complexes.
644 *Mol Cell Biol* **26**:2803-2816.

645 Fallini C, Bassell GJ, Rossoll W. 2012. Spinal muscular atrophy: the role of SMN in axonal
646 mRNA regulation. *Brain Res* **1462**: 81–92.

647 Fallini C, Zhang H, Su Y, Silani V, Singer RH, Rossoll W, Bassell GJ. 2011. The survival of
648 motor neuron (SMN) protein interacts with the mRNA-binding protein HuD and regulates
649 localization of poly(A) mRNA in primary motor neuron axons. *J Neurosci* **31**: 3914–3925.

650 Fischer U, Liu Q, Dreyfuss G. 1997. The SMN-SIP1 complex has an essential role in
651 spliceosomal snRNP biogenesis. *Cell* **90**: 1023–1029.

652 Frilander MJ, Steitz JA. 1999. Initial recognition of U12-dependent introns requires both U11/5'
653 splice-site and U12/branchpoint interactions. *Genes & development* **13**: 851-863.

654 Frugier T, Nicole S, Cifuentes-Diaz C, Melki J. 2002. The molecular bases of spinal muscular
655 atrophy. *Curr Opin Genet Dev* **12**: 294–298.

656 Gabanella F, Butchbach MER, Saieva L, Carissimi C, Burghes AHM, Pellizzoni L. 2007.
657 Ribonucleoprotein assembly defects correlate with spinal muscular atrophy severity and
658 preferentially affect a subset of spliceosomal snRNPs. *PLoS ONE* **2**: e921.

659 Hall SL, Padgett RA. 1994. Conserved sequences in a class of rare eukaryotic nuclear introns
660 with non-consensus splice sites. *J Mol Biol* **239**: 357–365.

661 Hoffman BE, Grabowski PJ. 1992. U1 snRNP targets an essential splicing factor, U2AF65, to
662 the 3' splice site by a network of interactions spanning the exon. *Genes & development* **6** :
663 2554-2568.

664 Jablonka S, Wiese S, Sendtner M. 2004. Axonal defects in mouse models of motoneuron disease.
665 *J Neurobiol* **58**: 272–286.

666 Jangi M, Fleet C, Cullen P, Gupta SV, Mekhoubad S, Chiao E, Allaire N, Bennett CF, Rigo F,
667 Krainer AR, et al. 2017. SMN deficiency in severe models of spinal muscular atrophy causes
668 widespread intron retention and DNA damage. *Proc Natl Acad Sci USA* **114**: E2347–E2356.

669 Kandels-Lewis S, Séraphin B. 1993. Involvement of U6 snRNA in 5' splice site selection.
670 *Science* **262** : 2035-2039.

671 Kashima T, Manley JL. 2003. A negative element in SMN2 exon 7 inhibits splicing in spinal
672 muscular atrophy. *Nat Genet* **34**: 460–463.

673 Kondo Y, Oubridge C, van Roon Am, Nagai K. 2015. Crystal structure of human U1 snRNP, a
674 small nuclear ribonucleoprotein particle, reveals the mechanism of 5' splice site recognition.
675 *eLife*. doi: 10.7554/eLife.04986.

676 Le TT, Pham LT, Butchbach MER, Zhang HL, Monani UR, Coover DD, Gavriline TO, Xing L,
677 Bassell GJ, Burghes AHM. 2005. SMNDelta7, the major product of the centromeric survival
678 motor neuron (SMN2) gene, extends survival in mice with spinal muscular atrophy and
679 associates with full-length SMN. *Hum Mol Genet* **14**: 845–857.

680 Lefebvre S, Bürglen L, Reboullet S, Clermont O, Burlet P, Viollet L, Benichou B, Cruaud C,
681 Millasseau P, Zeviani M. 1995. Identification and characterization of a spinal muscular
682 atrophy-determining gene. *Cell* **80**: 155–165.

683 Lefebvre S, Burlet P, Liu Q, Bertrand S, Clermont O, Munnich A, Dreyfuss G, Melki J. 1997.
684 Correlation between severity and SMN protein level in spinal muscular atrophy. *Nat Genet*
685 **16**: 265–269.

686 Lesser CF, Guthrie C. 1993. Mutations in U6 snRNA that alter splice site specificity:
687 implications for the active site. *Science* **262** : 1982-1988.

688 Lotti F, Imlach WL, Saieva L, Beck ES, Hao LT, Li DK, Jiao W, Mentis GZ, Beattie CE,
689 McCabe BD, et al. 2012. An SMN-dependent U12 splicing event essential for motor circuit
690 function. *Cell* **151**: 440–454.

691 McAndrew PE, Parsons DW, Simard LR, Rochette C, Ray PN, Mendell JR, Prior TW, Burghes
692 AH. 1997. Identification of proximal spinal muscular atrophy carriers and patients by analysis
693 of SMN2 and SMN1 gene copy number. *Am J Hum Genet* **60**: 1411–1422.

694 McConnell TS, Cho S-J, Frilander MJ, Steitz JA. 2002. Branchpoint selection in the splicing of
695 U12-dependent introns in vitro. *RNA* **8**: 579–586.

696 Meister G, Bühler D, Pillai R, Lottspeich F, Fischer U. 2001. A multiprotein complex mediates
697 the ATP-dependent assembly of spliceosomal U snRNPs. *Nat Cell Biol* **3**: 945–949.

698 Mercer TR, Clark MB, Andersen SB, Brunck ME, Haerty W, Crawford J, Taft RJ, Nielsen RK,
699 Dinger ME, Mattick JS. 2015. Genome-wide discovery of human splicing branchpoints.
700 *Genome research* **25** : 290-303.

701 Merendino L, Guth S, Bilbao D, Martínez C, Valcárcel J. 1999. Inhibition of msl-2 splicing by
702 Sex-lethal reveals interaction between U2AF35 and the 3' splice site AG. *Nature* **402** : 838-
703 841.

704 Michaud S, Reed R. 1993. A functional association between the 5' and 3' splice site is
705 established in the earliest prespliceosome complex (E) in mammals. *Genes & development* **7** :
706 1008-1020.

707 Michaud S, Reed R. 1991. An ATP-independent complex commits pre-mRNA to the
708 mammalian spliceosome assembly pathway. *Genes & development* **5** : 2534-2546.

709 Monani UR. 2005. Spinal muscular atrophy: a deficiency in a ubiquitous protein; a motor
710 neuron-specific disease. *Neuron* **48**: 885–896.

711 Montzka KA, Steitz JA. 1988. Additional low-abundance human small nuclear
712 ribonucleoproteins: U11, U12, etc. *Proc Natl Acad Sci USA* **85**: 8885–8889.

713 Moyer DC, Larue GE, Hershberger CE, Roy SW, Padgett RA. 2020. Comprehensive database
714 and evolutionary dynamics of U12-type introns. *Nucleic Acids Res* **48** : 7066-7078.

715 O'Brien K, Matlin AJ, Lowell AM, Moore MJ. 2008. The Biflavonoid Isoginkgetin Is a General
716 Inhibitor of Pre-mRNA Splicing. *J Biol Chem* **283** : 33147-33154.

717 Olthof AM, Hyatt KC, Kanadia RN. 2019. Minor intron splicing revisited: identification of new
718 minor intron-containing genes and tissue-dependent retention and alternative splicing of
719 minor introns. *BMC genomics* **20** : 686.

720 Olthof AM, White AK, Mieruszynski S, Dggett K, Lee MF, Chakroun A, Abdel Aleem AK,
721 Rousseau J, Magnani C, Roifman CM, Campeau PM, Heath JK, Kanadia RN. 2021.
722 Disruption of exon-bridging interactions between the minor and major spliceosomes results in
723 alternative splicing around minor introns. *Nucleic Acids Res* **49** : 3524-3545.

724 Pagliardini S, Giavazzi A, Setola V, Lizier C, Di Luca M, DeBiasi S, Battaglia G. 2000.
725 Subcellular localization and axonal transport of the survival motor neuron (SMN) protein in
726 the developing rat spinal cord. *Hum Mol Genet* **9**: 47–56.

727 Patel AA, McCarthy M, Steitz JA. 2002. The splicing of U12-type introns can be a rate-limiting
728 step in gene expression. *EMBO J* **21**: 3804–3815.

729 Paushkin S, Gubitza AK, Massenet S, Dreyfuss G. 2002. The SMN complex, an assemblysome
730 of ribonucleoproteins. *Curr Opin Cell Biol* **14**: 305–312.

731 Pearn J. 1978. Incidence, prevalence, and gene frequency studies of chronic childhood spinal
732 muscular atrophy. *J Med Genet* **15**: 409–413.

733 Pellizzoni L. 2007. Chaperoning ribonucleoprotein biogenesis in health and disease. *EMBO Rep*
734 **8**: 340–345.

735 Pellizzoni L, Baccon J, Charroux B, Dreyfuss G. 2001a. The survival of motor neurons (SMN)
736 protein interacts with the snoRNP proteins fibrillarin and GAR1. *Curr Biol* **11**: 1079–1088.

737 Pellizzoni L, Charroux B, Rappsilber J, Mann M, Dreyfuss G. 2001b. A functional interaction
738 between the survival motor neuron complex and RNA polymerase II. *J Cell Biol* **152**: 75–85.

739 Pellizzoni L, Kataoka N, Charroux B, Dreyfuss G. 1998. A novel function for SMN, the spinal
740 muscular atrophy disease gene product, in pre-mRNA splicing. *Cell* **95**: 615–624.

741 Pellizzoni L, Yong J, Dreyfuss G. 2002. Essential role for the SMN complex in the specificity of
742 snRNP assembly. *Science* **298**: 1775–1779.

743 Pessa HKJ, Ruokolainen A, Frilander MJ. 2006. The abundance of the spliceosomal snRNPs is
744 not limiting the splicing of U12-type introns. *RNA* **12**: 1883–1892.

745 Pomeranz Krummel DA, Oubridge C, Leung AK, Li J, Nagai K. 2009. Crystal structure of
746 human spliceosomal U1 snRNP at 5.5 Å resolution. *Nature* **458** : 475-480.

747 Query CC, Moore MJ, Sharp PA. 1994. Branch nucleophile selection in pre-mRNA splicing:
748 evidence for the bulged duplex model. *Genes Dev* **8**: 587–597.

749 Rage F, Boulisfane N, Rihan K, Neel H, Gostan T, Bertrand E, Bordonné R, Soret J. 2013.
750 Genome-wide identification of mRNAs associated with the protein SMN whose depletion
751 decreases their axonal localization. *RNA* **19**: 1755–1766.

752 Reed R. 1996. Initial splice-site recognition and pairing during pre-mRNA splicing. *Current*
753 *opinion in genetics & development* **6** : 215-220.

754 Rihan K, Antoine E, Maurin T, Bardoni B, Bordonné R, Soret J, Rage F. 2017. A new cis-acting
755 motif is required for the axonal SMN-dependent Anxa2 mRNA localization. *RNA* **23**: 899–
756 909.

757 Robberson BL, Cote GJ, Berget SM. 1990. Exon definition may facilitate splice site selection in
758 RNAs with multiple exons. *Molecular and cellular biology* **10** : 84-94.

759 Roesser JR. 2004. Both U2 snRNA and U12 snRNA are required for accurate splicing of exon 5
760 of the rat calcitonin/CGRP gene. *RNA* **10**: 1243–1250.

761 Rossoll W, Jablonka S, Andreassi C, Kröning A-K, Karle K, Monani UR, Sendtner M. 2003.
762 Smn, the spinal muscular atrophy-determining gene product, modulates axon growth and
763 localization of beta-actin mRNA in growth cones of motoneurons. *J Cell Biol* **163**: 801–812.

764 Ruskin B, Zamore PD, Green MR. 1988. A factor, U2AF, is required for U2 snRNP binding and
765 splicing complex assembly. *Cell* **52** : 207-219.

766 Schrank B, Götz R, Gunnensen JM, Ure JM, Toyka KV, Smith AG, Sendtner M. 1997.
767 Inactivation of the survival motor neuron gene, a candidate gene for human spinal muscular
768 atrophy, leads to massive cell death in early mouse embryos. *Proc Natl Acad Sci USA* **94**:
769 9920–9925.

770 Sendtner M. 2001. Molecular mechanisms in spinal muscular atrophy: models and perspectives.
771 *Curr Opin Neurol* **14**: 629–634.

772 Sharp PA, Burge CB. 1997. Classification of introns: U2-type or U12-type. *Cell* **91** : 875-879.

773 Shen H, Zheng X, Luecke S, Green MR. 2010. The U2AF35-related protein Urp contacts the 3'
774 splice site to promote U12-type intron splicing and the second step of U2-type intron splicing.
775 *Genes & development* **24** : 2389-2394 ;

776 Sumner CJ. 2006. Therapeutics development for spinal muscular atrophy. *NeuroRx* **3**: 235–245.

777 Taggart AJ, Lin CL, Shrestha B, Heintzelman C, Kim S, Fairbrother WG. 2017. Large-scale
778 analysis of branchpoint usage across species and cell lines. *Genome research* **27** : 639-649.

779 Talbot K, Davies KE. 2001. Spinal muscular atrophy. *Semin Neurol* **21**: 189–197.

780 Turunen JJ, Niemelä EH, Verma B, Frilander MJ. 2013. The significant other: splicing by the
781 minor spliceosome. *Wiley Interdiscip Rev RNA*. **4**:61-76.

782 Verma B, Akinyi MV, Norppa AJ, Frilander MJ. 2018. Minor spliceosome and disease.
783 *Seminars in cell & developmental biology* **79** : 103-112.

784 Wan L, Battle DJ, Yong J, Gubitzi AK, Kolb SJ, Wang J, Dreyfuss G. 2005. The survival of
785 motor neurons protein determines the capacity for snRNP assembly: biochemical deficiency
786 in spinal muscular atrophy. *Mol Cell Biol* **25**: 5543–5551.

787 Wang J, Dreyfuss G. 2001. A cell system with targeted disruption of the SMN gene: functional
788 conservation of the SMN protein and dependence of Gemin2 on SMN. *J Biol Chem* **276**:
789 9599–9605.

790 Wassarman KM, Steitz JA. 1992. The low-abundance U11 and U12 small nuclear
791 ribonucleoproteins (snRNPs) interact to form a two-snRNP complex. *Molecular and cellular*
792 *biology* **12** : 1276-1285.

793 Whitehead SE, Jones KW, Zhang X, Cheng X, Terns RM, Terns MP. 2002. Determinants of the
794 interaction of the spinal muscular atrophy disease protein SMN with the dimethylarginine-
795 modified box H/ACA small nucleolar ribonucleoprotein GAR1. *J Biol Chem* **277**: 48087–
796 48093.

797 Wu JY, Maniatis T. 1993. Specific interactions between proteins implicated in splice site
798 selection and regulated alternative splicing. *Cell* **75** : 1061-1070.

799 Wu Q, Krainer AR. 1996. U1-mediated exon definition interactions between AT-AC and GT-
800 AG introns. *Science* **274** : 1005-1008.

801 Wu S, Romfo CM, Nilsen TW, Green MR. 1999. Functional recognition of the 3' splice site AG
802 by the splicing factor U2AF35. *Nature* **402** : 832-835.

803 Xu YZ, Query CC. 2007. Competition between the ATPase Prp5 and branch region-U2 snRNA
804 pairing modulates the fidelity of spliceosome assembly. *Molecular cell* **28** : 838-849.

805 Zhang HL, Pan F, Hong D, Shenoy SM, Singer RH, Bassell GJ. 2003. Active transport of the
806 survival motor neuron protein and the role of exon-7 in cytoplasmic localization. *J Neurosci*
807 **23**: 6627–6637.

808 Zhang Z, Lotti F, Dittmar K, Younis I, Wan L, Kasim M, Dreyfuss G. 2008. SMN deficiency
809 causes tissue-specific perturbations in the repertoire of snRNAs and widespread defects in
810 splicing. *Cell* **133**: 585–600.

811 Zorio Da, Blumenthal T. 1999. Both subunits of U2AF recognize the 3' splice site in
812 *Caenorhabditis elegans*. *Nature* **402** : 835-838.
813

814 LEGENDS FOR FIGURES

815 **Figure 1:** Differential splicing of minor introns in spinal cords of SMA mice. (A) RT-PCR
816 analysis of minor introns splicing in spinal cords of control (WT6, WT7) and SMA (KO6,
817 KO9, KO10) mice. Three examples of retained introns are shown. Gene names and size (in
818 base pairs) of the amplified products are indicated on the left. The schematic structure of the
819 amplified products is shown on the right. (B) RT-PCR analysis of minor introns splicing in
820 spinal cords of control (WT6, WT7) and SMA (KO6, KO9, KO10) mice. Three examples of
821 unaffected introns are shown. (C) Retention index of minor introns in spinal cords of control
822 (WT, n=2) and SMA (SMA, n=3) mice determined as described in the *Materials and Methods*
823 section. Mean and SEM are shown. Statistical significance was calculated using the student *t*-
824 test (ns: non significant; * : *P* value < 0.05). Histograms for Ppp2r2b and 2c are not shown
825 because retained introns are not detectable.

826

827 **Figure 2:** The sequence of the splice donor site is not a key determinant of minor intron
828 retention in spinal cords of SMA mice. RT-PCR analysis of minor introns splicing in spinal
829 cords of control (WT6, WT7) and SMA (KO6, KO9, KO10) mice. (A) Unaffected minor
830 introns containing canonical 5' splice site sequences. (B) Retained minor introns containing
831 canonical 5' splice site sequences. (C) Unaffected minor introns containing suboptimal 5'
832 splice site sequences. Nucleotides diverging from the consensus are underlined. (D) Retained
833 minor introns containing suboptimal 5' splice site sequences. Nucleotides diverging from the
834 consensus are underlined. Gene names and size (in base pairs) of the amplified products are
835 indicated on the left. The schematic structure of the amplified products is shown on the right.
836 (E) Retention index of minor introns in spinal cords of control (WT, n=2) and SMA (SMA,
837 n=3) mice determined as described in the *Materials and Methods* section. Mean and SEM are
838 shown. Statistical significance was calculated using the student *t*-test (ns: non significant; * :
839 *P* value < 0.05; ** : *P* value < 0.01; *** : *P* value < 0.005). Histograms for Mapk1 and Ncbp2
840 are not shown because retained introns are not or hardly detectable.

841

842 **Figure 3:** Branchpoint sequence is a key determinant of minor intron retention in spinal cord
843 of SMA mice. RT-PCR analysis of minor introns splicing in spinal cords of control (WT6,
844 WT7) and SMA (KO6, KO9, KO10) mice. (A) Minor introns containing canonical
845 branchpoint sequences. (B) Minor introns containing suboptimal branchpoint sequences.
846 Nucleotides diverging from the consensus are underlined. The putative branchsite adenosine
847 is indicated in bold. The branchpoint sequence is aligned with the anti-branch site of the U12
848 snRNA (in italics). Gene names and size (in base pairs) of the amplified products are
849 indicated on the left. The schematic structure of the amplified products is shown on the
850 right.(C) Retention index of minor introns in spinal cords of control (WT, n=2) and SMA
851 (SMA, n=3) mice determined as described in the *Materials and Methods* section. Mean and
852 SEM are shown. Statistical significance was calculated using the student *t*-test (ns: non
853 significant; **: *P* value < 0.01). Histograms for Ddx54 and Ppp2r2b are not shown because
854 retained intron is not detectable.

855 **Figure 4:** The score of the branchpoint sequence is correlated to the splicing efficiency of
856 most minor introns. RT-PCR analysis of minor introns splicing in spinal cords of control
857 (WT6, WT7) and SMA (KO6, KO9, KO10) mice. Gene names and size (in base pairs) of the
858 amplified products are indicated on the left. The schematic structure of the amplified products
859 is shown on the right. The branchpoint sequence aligned with the anti-branch site of the U12
860 snRNA (in italics) as well as the BPS scores are shown on the right. The putative branchsite
861 adenosine is indicated in bold. (A) Minor introns containing canonical branchpoint sequences.
862 (B) Minor introns containing suboptimal branchpoint sequences. (C) Retention index of
863 minor introns in spinal cords of control (WT, n=2) and SMA (SMA, n=3) mice determined as
864 described in the *Materials and Methods* section. Mean and SEM are shown. Statistical
865 significance was calculated using the student *t*-test (ns: non significant; * : *P* value < 0.05; **
866 : *P* value < 0.01). Histograms for *Srpk1* are not shown because retained introns are not
867 detectable.

868

869 **Figure 5:** Splicing of a subset of minor introns containing suboptimal BPS is not affected in
870 spinal cords of SMA mice. RT-PCR analysis of minor introns splicing efficiency in spinal
871 cords of control (WT6, WT7) and SMA (KO6, KO9, KO10) mice. Gene names and size (in
872 base pairs) of the amplified products are indicated on the left. The schematic structure of the
873 amplified products is shown on the right. The branchpoint sequence aligned with the anti-
874 branch site of the U12 snRNA (in italics) as well as the U12 BPS scores are shown on the
875 right. The putative branchsite adenosine is indicated in bold. Minor introns with low BPS
876 scores are retained (A) or not affected (B) in spinal cords of SMA mice. (C) Retention index
877 of minor introns in spinal cords of control (WT, n=2) and SMA (SMA, n=3) mice determined
878 as described in the *Materials and Methods* section. Mean and SEM are shown. Statistical
879 significance was calculated using the student *t*-test (ns: non significant; * : *P* value < 0.05; **
880 : *P* value < 0.01). Histograms for *Gosr1* are not shown because retained intron is not
881 detectable.

882

883 **Figure 6:** Schematic representation of the reporters used for *in vitro* splicing experiments.
884 The name of the corresponding gene, the U12 and U2 scores of the minor introns and the size
885 of the exons and introns are indicated. Exonic sequences (grey boxes), minor splicing signals
886 (splice donor, branchpoint sequence and splice acceptor), as well as downstream sequences
887 containing the major splice donor site are in capital letters.

888

889 **Figure 7:** The U2 snRNP participates to the splicing of the *Tsta3* minor intron in the presence
890 of functional U12 snRNPs. (A) Representative gel of RT-PCR experiments analyzing
891 simultaneously the amount of unspliced and spliced products obtained with the different
892 reporters. Reporter names and size (in base pairs) of the amplified products are indicated on
893 the left and the schematic structure of the splicing products is shown on the right.
894 Preincubation of the splicing extracts with LNAs targeting the U2 (U2, 2 μ M), U12 (U12,
895 2nM) or U12 + U2 snRNAs is indicated. The faint band detected immediately below the

896 Slc12a4 and Vac14 unspliced products likely corresponds to a spliced-unspliced heteroduplex
897 RNA (B) Splicing efficiency (in %) determined for the different reporter substrates following
898 incubation in control (Ctl) or LNA-pre-treated extracts. (C) Representative gel of RT-PCR
899 experiments analyzing simultaneously the amount of unspliced and spliced products obtained
900 with the Slc12a4 and Tsta3 reporters. Preincubation of the splicing extracts with LNAs
901 targeting the U2 (U2, 2 μ M) or U12 (U12, 2 μ M) snRNAs is indicated. (D) Splicing efficiency
902 (in %) determined for the different reporter substrates following incubation in control (Ctl) or
903 LNA-pre-treated extracts. Statistical significance was calculated using the student *t*-test (n=3;
904 * : *P* value < 0.05; **: *P* value < 0.01; ***: *P* value < 0.001; ****: *P* value < 0.0001).

905

906 **Figure 8:** The Plcb3 minor intron contains competing BPSs differentially affected by U2
907 depletion. (A) Schematic representation of the Plcb3 splicing reporter and electrophoregram
908 indicating the alternative 3' splice site used to generate the 127 nt mRNA. The U12 and U2
909 scores of the competing branchsites and the size of the exons and introns are indicated.
910 Exonic sequences (grey boxes), minor splicing signals (splice donor, branchpoint sequence
911 and splice acceptor), as well as downstream sequences containing the major splice donor site
912 are in capital letters. (B) Representative gel of RT-PCR experiments analyzing simultaneously
913 the amount of unspliced and spliced products obtained with the Plcb3 reporter. Preincubation
914 of the splicing extracts with LNAs targeting the U2 (U2, 2 μ M), U12 (U12, 2nM) or U12 + U2
915 snRNAs is indicated. The schematic structure of the splicing products is shown on the right
916 and the size (in base pairs) is indicated on the left. (C) Splicing efficiency (in %) determined
917 for the different splicing products following incubation in control (Ctl) or LNA-pre-treated
918 extracts. "Alt" refers to the 127 nt long mRNA. Statistical significance was calculated using
919 the student *t*-test (n=3; ns: non significant; * : *P* value < 0.05; **: *P* value < 0.01; ***: *P*
920 value < 0.001).

921

922 **Figure 9:** The branchpoint sequence is responsible for the Tsta3 splicing dependence on U2
923 snRNP. (A) Representative gel of RT-PCR experiments analyzing simultaneously the amount
924 of unspliced and spliced products obtained with the Tsta3 reporter with different branchpoint
925 sequences. Reporter names and size (in base pairs) of the amplified products are indicated on
926 the left. The schematic structure of the splicing products is shown on the right. Preincubation
927 of the splicing extracts with LNAs targeting the U2 (U2, 2 μ M), U12 (U12, 2nM) or U12 + U2
928 snRNAs is indicated. (B) Schematic representation and electrophoregram indicating the major
929 cryptic splice sites activated in the Tsta3 BPS Slc12a4 reporter following partial inactivation
930 of the U12 snRNPs. (C) (D) Splicing efficiency (in %) determined for the Tsta3 BPS Slc12a4
931 (C) and Tsta3 BPS Mapk1 (D) reporter substrates following incubation in control (Ctl) or
932 LNA-pre-treated extracts. In (C) Min refers to the regular splicing event and Maj to the
933 cryptic one. (E) Representative gel of RT-PCR experiments analyzing simultaneously the
934 amount of unspliced and spliced products obtained with the Tsta3 BPS Mapk1 reporter.
935 Preincubation of the splicing extracts with LNAs targeting the U12 (U12, 2 μ M) snRNAs is
936 indicated. (F) Splicing efficiency (in %) determined for the Tsta3 BPS Mapk1 following

937 incubation in control (Ctl) or LNA-pre-treated extracts. Statistical significance was calculated
938 using the student *t*-test (n=3; *: *P* value < 0.05; **: *P* value < 0.01; ***: *P* value < 0.001;
939 ****:*P* value <0.0001).

940

941 **Figure 10:** The Tsta3 branchpoint sequence efficiently interacts with the U2 snRNA. (A)
942 Representative gels of RT-PCR experiments analyzing the amount of U12 and U2 snRNAs
943 binding to the beads alone (Control Beads), to the reporter RNAs without the UV crosslinking
944 step or crosslinked to the Tsta3 (1) or Tsta3 BPS Slc12a4 (2) reporter pre-mRNAs. PCR
945 reactions specific for sequences of the 3' exon present in both reporters (E2) was used to
946 normalize for affinity purification efficiency. The size (in base pairs) of the amplified
947 fragments is indicated. (B) Relative enrichment of U12 and U2 snRNAs obtained with the
948 control beads (CB) and with the Tsta3 (1) or Tsta3 BPS Slc12a4 (2) reporter pre-mRNAs. For
949 each snRNA, the intensities (expressed in arbitrary units) were normalized using the signal
950 obtained with primers specific for the Tsta3 3' exon (E2) as a reference. Statistical
951 significance was calculated using the student *t*-test (n=4; **: *P* value < 0.01). (C) Semi
952 quantitative RT-PCR analyses of U2 snRNA amounts copurified with the Tsta3 (1) or Tsta3
953 BPS Slc12a4 (2) reporter pre-mRNAs after UV crosslinking. PCR reactions specific for
954 sequences of the 3' exon present in both reporters (E2) and used to normalize for affinity
955 purification efficiency of the Tsta3 (1) or Tsta3 BPS Slc12a4 (2) reporter pre-mRNAs are
956 shown. The size of the amplified fragments is the same as in (A). The number of PCR cycles
957 is indicated on the left. (D) Quantification of the PCR products shown in (C). (E) Relative
958 enrichment of U2 snRNA in UV crosslinking experiments performed with the Tsta3 (1) or
959 Tsta3 BPS Slc12a4 (2) reporter pre-mRNAs. The intensities (expressed in arbitrary units)
960 were normalized using the signal obtained with primers specific for the Tsta3 3' exon (E2) as
961 a reference (n=2).

962

963 **Figure 11:** Time course analyses of splicing reactions performed with the Tsta3 or Tsta3 BPS
964 Slc12a4 reporter pre-mRNAs. (A) Time course analysis of the Tsta3 or Tsta3 BPS Slc12a4
965 pre-mRNAs splicing was performed at 0, 5, 10, 15 and 20 minutes time points (Left panels)
966 and at 0, 20, 40, 60, 80 and 100 minutes time points (Right panels). Splicing products were
967 separated in 4% denaturing polyacrylamide gels. The schematic structure of the splicing
968 products is indicated. (B) and (C) Splicing efficiency (in %) of the Tsta3 and Tsta3 BPS
969 Slc12a4 pre-mRNAs (n=2).

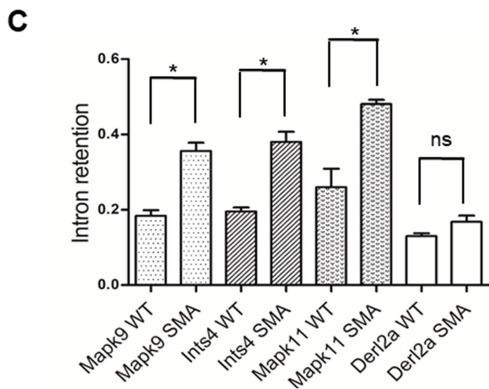
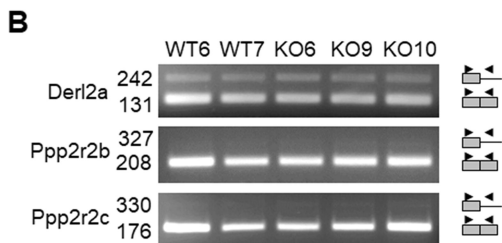
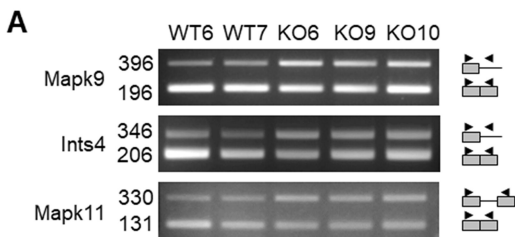
970

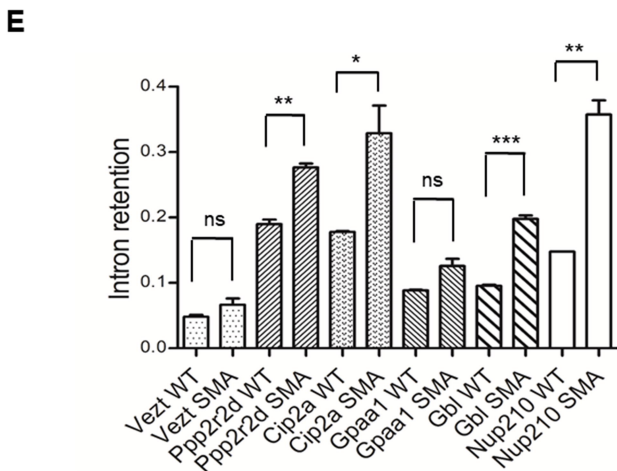
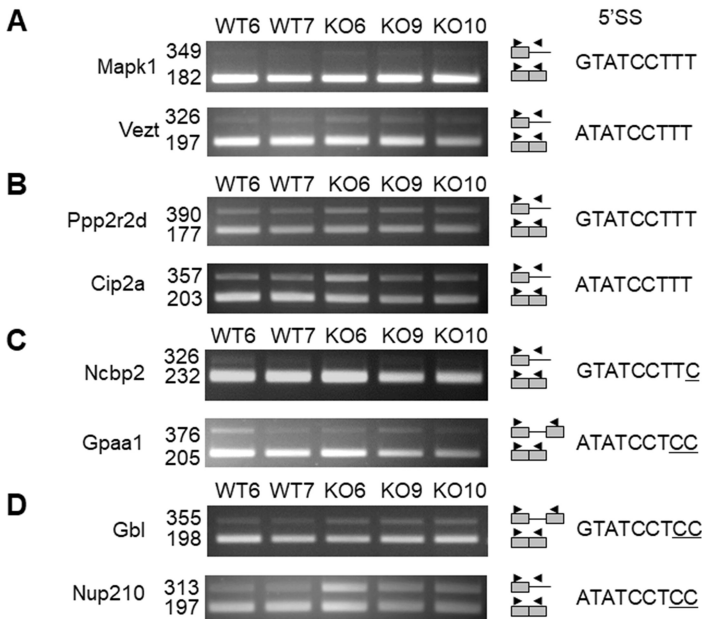
971 **Figure 12:** Alternative models for U2 snRNP involvement in the splicing of a subset of minor
972 introns. (A) Schematic representation of putative interactions between the U2 and U12
973 snRNPs. These interactions could be either direct or involve additional factor(s) related
974 (Zrsr2) or not to the U2AF complex. The 65K protein involved in the bridging of the U11 and
975 U12 snRNPs is shown. The exon definition model accounting for the need of a major 5'
976 splice site for efficient splicing of the upstream minor intron (Wu and Krainer 1996) is also
977 depicted. (B) Schematic representation of putative interactions between the U2 and U11

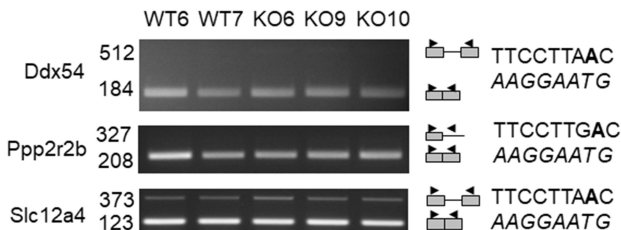
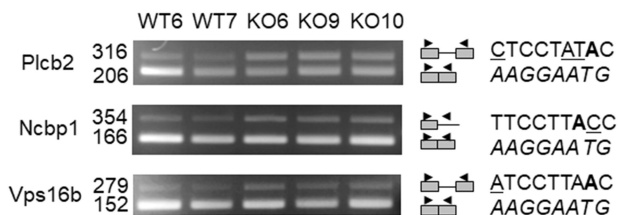
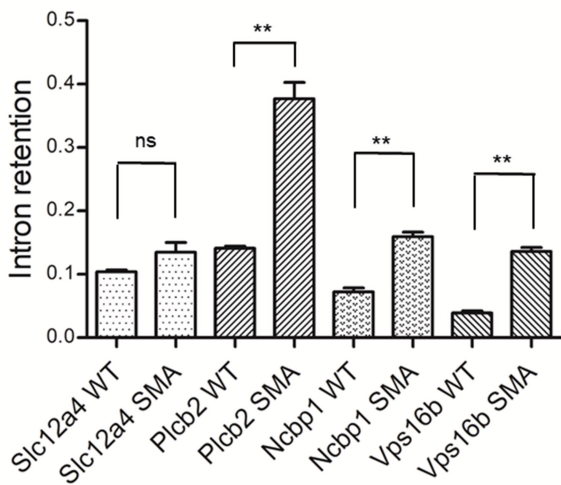
978 snRNPs. These interactions could involve the 59K protein of the U11 snRNP and components
979 of the U2 snRNP such as SF3B1, as recently proposed (Olthof et al. 2021).

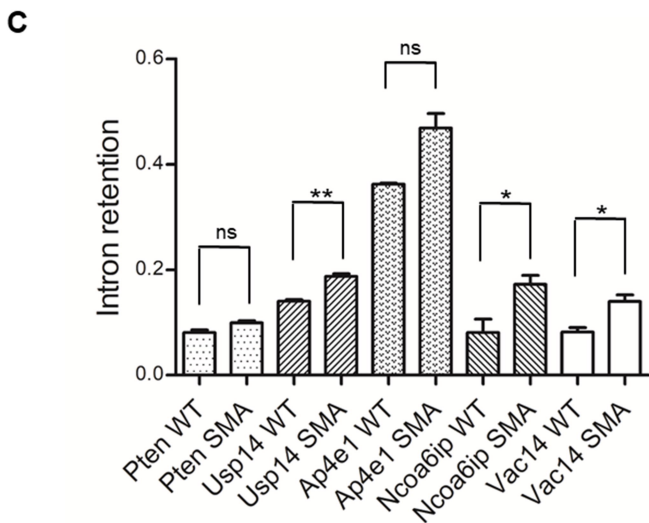
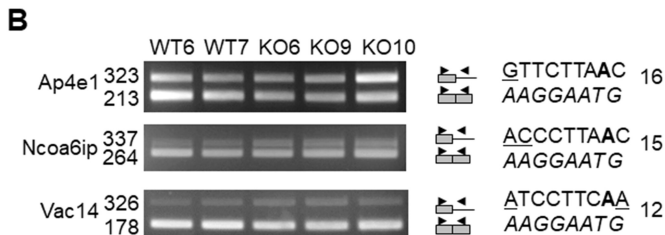
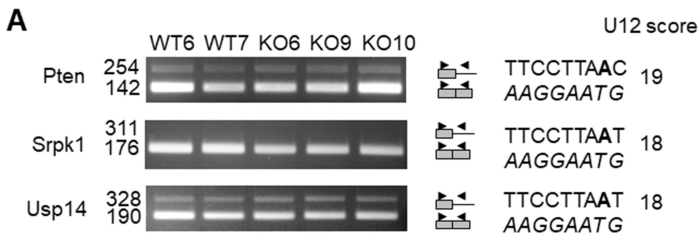
980

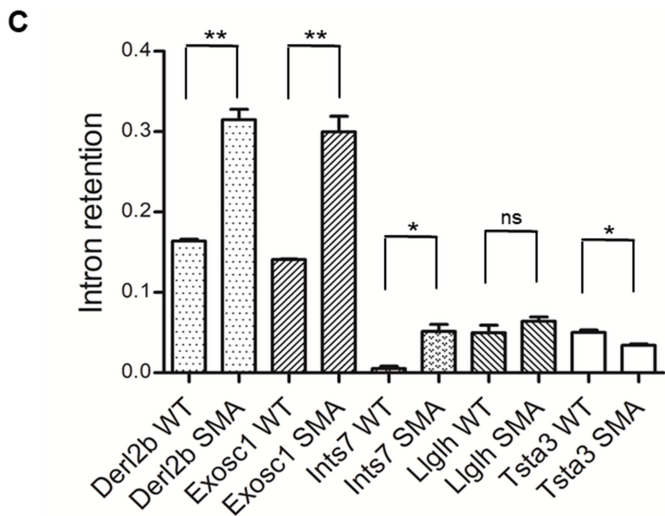
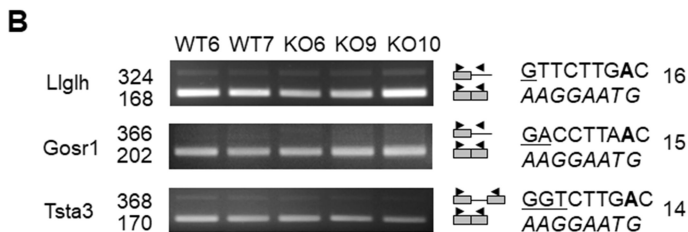
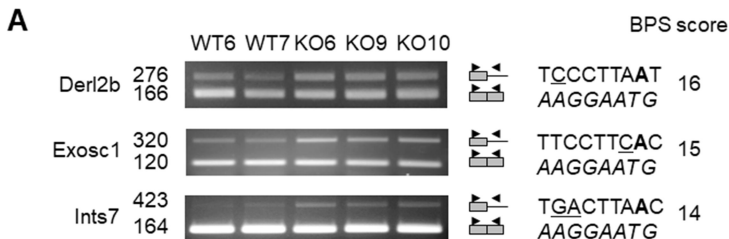
981 **Table 1:** Features of murine minor introns used in this study. Intron Id and gene name are
982 from the U12DB (Alioto 2007). The Branchpoint (BP) sequences and their corresponding
983 U12 and U2 H Bonds scores are indicated. Intron retention fold change in the spinal cord of
984 SMA mice and corresponding *P* values are shown (na: not applicable; ns: not significant; * :
985 *P* value < 0.05; **: *P* value < 0.01; ***: *P* value < 0.001).



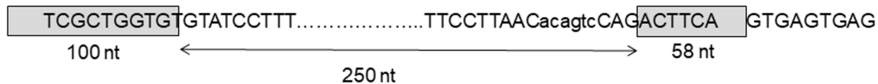


A**B****C**

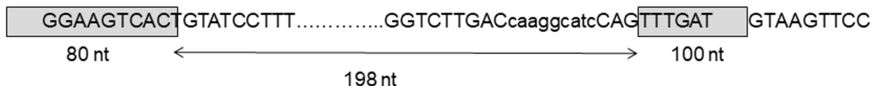




Slc12a4 : U12=19; U2=9



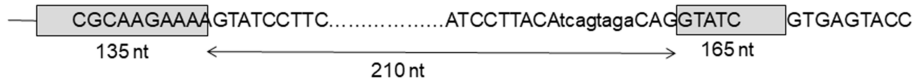
Tsta3 : U12=14; U2=16

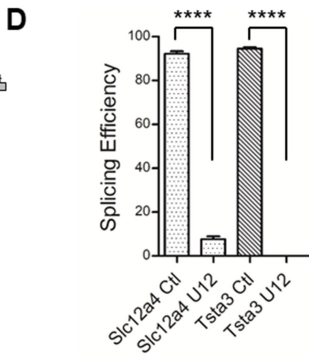
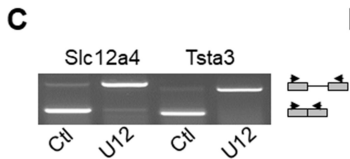
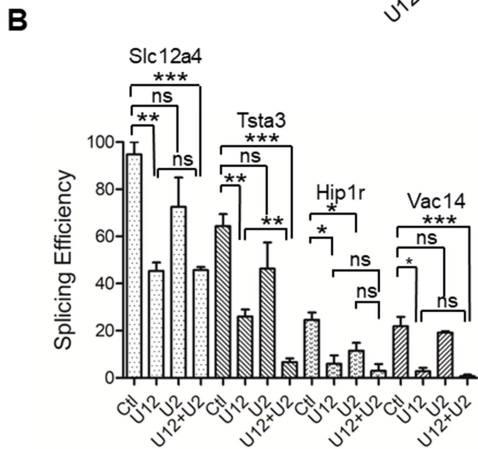
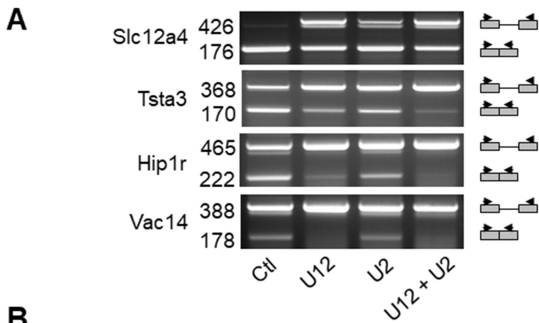


Hip1r : U12=15; U2=14



Vac14 : U12=12; U2=4



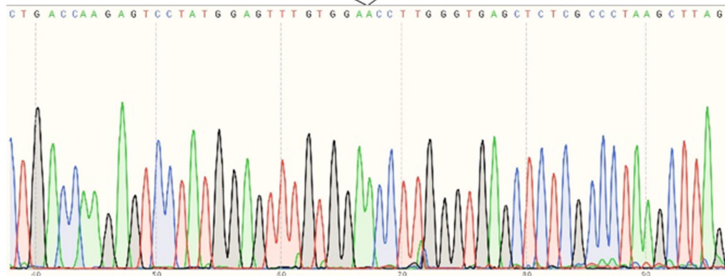
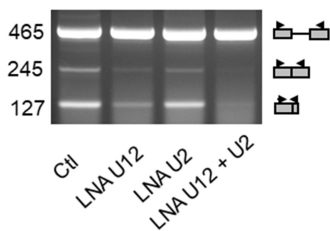
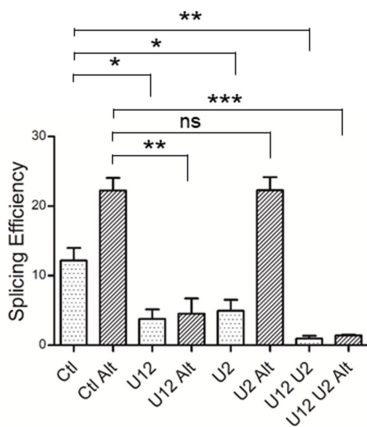


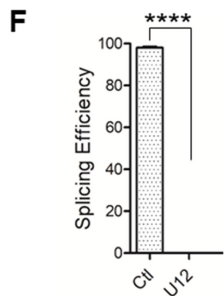
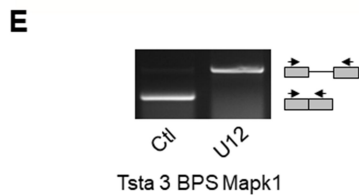
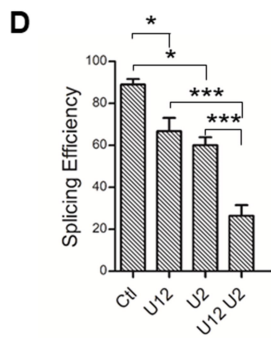
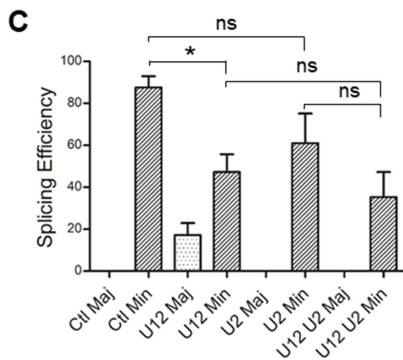
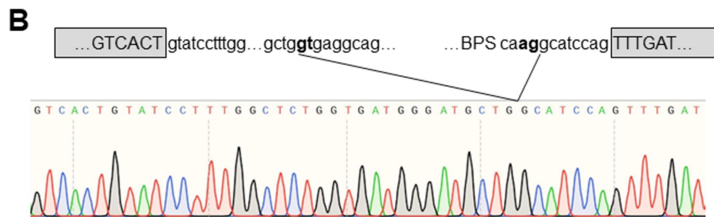
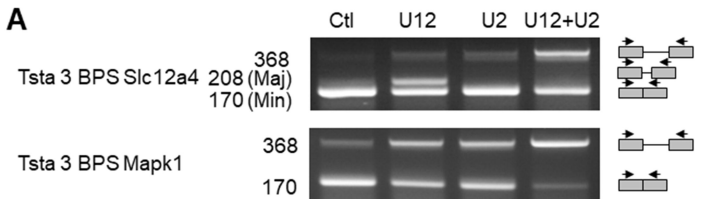
A

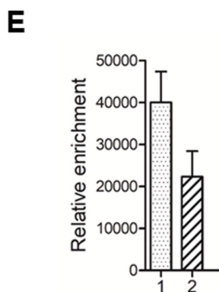
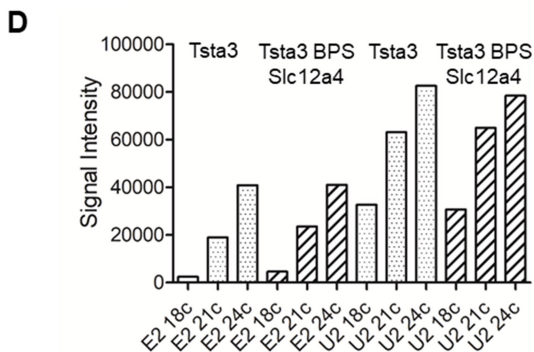
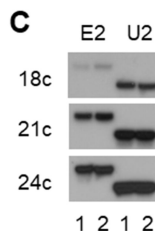
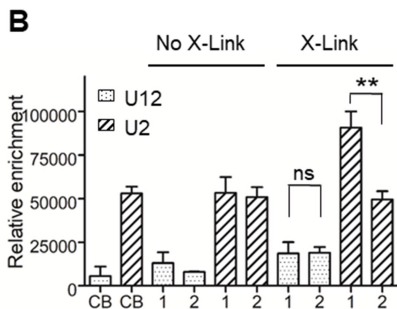
Plcb3: U12=13; U2=15

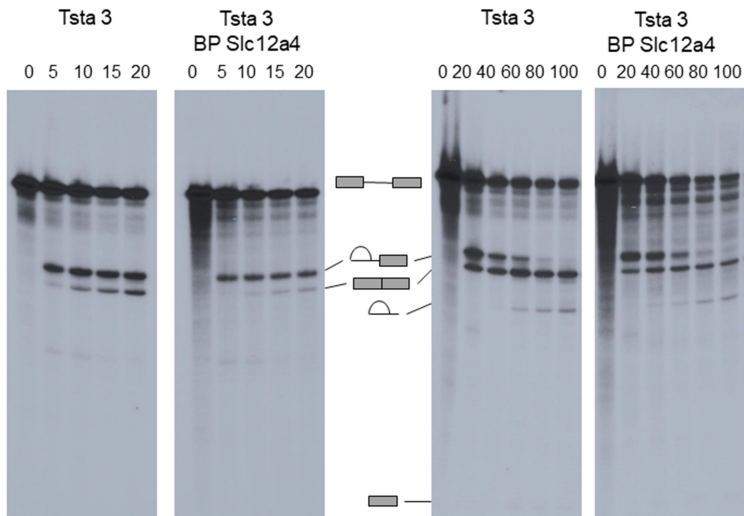
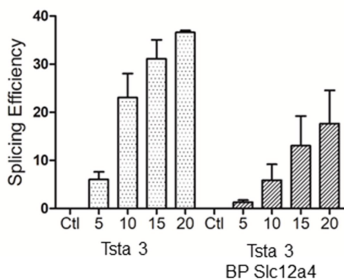
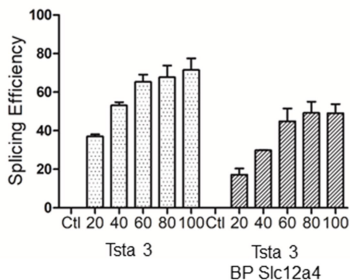


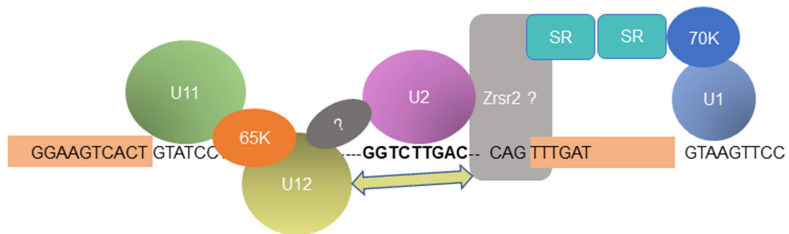
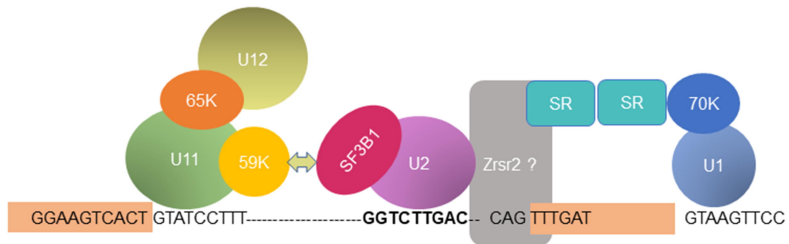
Plcb3 Alt: U12=13; U2=10

**B****C**





A**B****C**

A**B**

Intron Id	Gene Name	BP Sequence	H Bonds U12	H Bonds U2	Retention fold change	Pval	Figure
26845	Derl2a	UUCCUUAAC	19	9	1,29	ns	1
24328	Ppp2r2b	UUCCUUGAC	19	9	1	na	1
24323	Ppp2r2c	UUCCUUGAC	19	9	1	na	1
28907	Mapk11	UUCCUGGAC	17	7	1,85	*	1
30182	Mapk9	UUCCUCAAG	14	4	1,94	*	1
24751	2610034N24Rik/Ints4	CCACUUAAC	12	9	1,94	*	1
29557	Ncbp2	UUCCUUAAC	19	9	1	na	2
31297	Gpaa1	GUCCUUGAC	17	12	1,08	ns	2
24310	Ppp2r2d	UGCCUUAAC	17	11	1,46	**	2
26419	Gbl	AUCCUUAAC	17	9	2,07	***	2
29204	C330027C09Rik/Cip2a	UAUCUUAAC	16	13	1,68	*	2
28929	Nup210	UACCUUAAU	16	10	2,42	**	2
26577	Mapk1	GACCUUAAC	15	14	1	na	2
25128	AI854408 vezt	GGCCUUAAC	15	14	1,38	ns	2
25193	Ddx54	UUCCUUAAC	19	9	1	na	3
26106	Slc12a4	UUCCUUAAC	19	9	1,3	ns	3
28406	Vps16	AUCCUUAAC	17	9	3,5	**	3
31448	AU014645/Ncbp1	UUCCUUCAC	17	7	2,21	**	3
26159	Plcb2	CUCCUAUAC	13	5	2,67	**	3
24088	Pten	UUCCUUAAC	19	9	1,22	ns	4
30287	Srpk1	UUCCUAAU	18	8	1	na	4
27284	Usp14	UUCCUAAU	18	8	1,33	**	4
26255	Ap4e1	GUUCUUAAC	16	14	1,3	ns	4
31136	Ncoa6ip	ACCCUUAAC	15	9	2,13	*	4
26739	Vac14	AUCCUCAA	12	4	1,71	*	4
26953	Llglh	GUUCUUGAC	16	14	1,28	ns	5
26818	Derl2b	UCCCUUAAU	16	8	1,92	**	5
27023	Gosr1	GACCUUAAC	15	14	1	na	5
24183	Exosc1	UCCCUUCAC	15	7	2,13	**	5
31292	Tsta3	GGUCUUGAC	14	16	0,67	*	5
23814	5930412E23Rik/Ints7	UGACUUAAC	14	11	9,63	*	5